Article

6-Aminocoumarin-Naphthoquinone Conjugates: Design, Synthesis, Photophysical and Electrochemical Properties and DFT Calculations

Fabio S. Miranda,* Célia M. Ronconi, Mikaelly O. B. Sousa,
Gleiciani Q. Silveira and Maria D. Vargas*

Instituto de Química, Universidade Federal Fluminense,
Campus do Valonguinho, Centro, 24020-141 Niterói-RJ, Brazil

Quatro novos conjugados do tipo 6-aminocumarina-naftoquinona foram sintetizados e suas propriedades fotofísicas e eletroquímicas, investigadas. O composto 2-cloro-3-(2-oxo-2H-cromen-6-ilamino)-1,4-naftoquinona **1** não apresentou fluorescência apreciável, em comparação com a 6-aminocumarina, 6-AC. Visando entender as razões da extinção da fluorescência neste composto, duas estratégias foram imaginadas. Primeiramente, o composto **1** foi metilado no nitrogênio para remover a interação eletrostática intramolecular N-H…O=C que mantém as duas unidades fixas. Entretanto, as propriedades de emissão do produto **2** não se mostraram significantemente diferentes das do precursor **1**. Como os cálculos usando a teoria do funcional da densidade dependente do tempo (TD-DFT) dos compostos **1** e **2** indicaram que a supressão da fluorescência relaciona-se ao caráter aceptor no anel naftoquinônico, a segunda estratégia envolveu a substituição do átomo de cloro na posição 2 do núcleo naftoquinônico por diferentes grupos doadores de elétrons (compostos **3**-**5**). Novamente não houve mudanças apreciáveis nas propriedades de emissão. Para explicar estes resultados foram feitos cálculos TD-DFT dos estados fundamental (S_0) e excitado (S_1) de todas as moléculas em solução, os quais indicaram que o grupo fluorescente (6-AC) doa elétrons para o LUMO da naftoquinona, resultando em uma transferência de elétron fotoinduzida oxidativa (*oxidative-PET*).

Four novel 6-aminocoumarin-naphthoquinone conjugates were synthesized and their photophysical and electrochemical properties, investigated. 2-Chloro-3-(2-oxo-2H-chromen-6-ylamino)-1,4-naphthoquinone **1** did not present appreciable fluorescence in solution in comparison with 6-aminocoumarin, 6-AC. In order to understand the reasons for the fluorescence quenching in this compound, two strategies were attempted. Firstly, compound **1** was *N*-methylated to remove the intramolecular N-H…O=C electrostatic interaction that maintained the two units fixed, but the emission properties of the product **2** were not significantly different from those of **1**. Time-dependent density functional theory (TD-DFT) calculations of compounds **1** and **2** indicate that the fluorescence quenching is related to the electron acceptor character of the naphthoquinone ring. The second strategy, therefore, involved the substitution of the chlorine atom in position 2 of the naphthoquinone nucleus for different electron donor groups (compounds **3**-**5**), but again the emission properties did not change significantly. To explain these experimental findings, TD-DFT calculations of the ground (S_0) and excited (S_1) states of all molecules in solution were carried out. The results suggest that the energy states in these conjugates are such that the fluorescent group (6-AC) donates electrons to the naphthoquinone LUMO resulting in an oxidative photoinduced electron transfer (oxidative-PET).

Keywords: aminonaphthoquinone, aminocoumarin, TD-DFT calculations, fluorescence

Introduction

2-Amino-1,4-naphthoquinones are known for their various biological activities, e.g., antitumor,[1-4] molluscicidal,[5,6] antiparasitic,[7] antimicrobial,[8] pesticide[9] and herbicidal,[10] among others.[11] These properties have been related to the ability of quinones to accept one or two electrons with formation of the respective radical-anion or dianion. Judicious choice of the substituents either on position 3 of the quinone ring or on the nitrogen atom

*e-mail: miranda@vm.uff.br, mdvargascp@gmail.com

allows modulation of the redox,[12,13] acid-base, solubility and pharmacological properties.[14,15]

In recent years the use of fluorescent probes attached to biologically active molecules has attracted great interest in the field of medical and biological research.[16,17] Labelling agents allow a better understanding of drug accumulation and interaction with the target, e.g., tumor cell, by monitoring the fluorescence signals.[18] Several organic dyes have been used as fluorescent probes, e.g., fluorescein, coumarin, rhodamine,[19] cyanine, and Alexa dyes.[20] Among those, coumarins are interesting not only because of their fluorescence, but also because of their pharmacological activities.[21] 6-Aminocoumarin (6-AC) - a molecule containing a donor amine group and an acceptor lactone ring - is a probe of choice because it can be easily prepared and coupled to biologically active molecules through nucleophilic substitution reactions. In addition 6-AC fluorescence quantum yield and fluorescence decay time can be modulated by changing the solvent polarity.[22,23]

In the present study we have investigated the possibility of incorporating the 6-AC fluorescent dye into a 1,4-naphthoquinone nucleus by reaction with 2,3-dichloro-1,4-naphthoquinone (DCN). Only a few examples of molecules containing both coumarin and 1,4-naphthoquinone nuclei have been described in the literature, mostly from natural sources.[24-27] Our hypothesis was that this conjugate would be fluorescent enough to allow fluorescence microscopy studies in the course of our further biological activity investigations. Instead, however, quenching was observed. In order to understand this process the photophysical and electrochemical properties of a series of 2-aminocoumarin-naphthoquinone conjugates (see Scheme 1) have been studied and interpreted with the help of density functional theory (DFT) calculations.

## Results and discussion

Syntheses of the compounds

The synthetic routes to compounds **1-5** are outlined in Scheme 1. Compound **1** was obtained from the reaction of 6-AC with DCN, which has been used as the starting material for the synthesis of a number of N-, S- and O-substituted derivatives.[9,15,27-30] *N*-methylation of **1** following procedure previously described[31] yielded compound **2** in good yields. Further substitution of a chloride group with propanethiol, thiophenol or 4-chlorothiophenol in the presence of Et$_3$N gave compounds **3**, **4** and **5**, respectively in 64-82% yields. Novel compounds **2-5** had their purity confirmed by elemental analyses and melting point measurements, and were characterized by ^{1}H and ^{13}C nuclear magnetic resonance (NMR) and Fourier transform infrared (FTIR) spectroscopy (see Figures S1-S18 in the SI section). The X-ray molecular structure of **1** has been reported previously.[32]

Photophysical properties

The normalized UV-Vis absorption and emission spectra of all aminocoumarin-napthoquinone conjugates in CH$_3$CN are shown in Figure 1.

The UV-Vis spectra of compounds **1-5** exhibit four absorption bands: a high energy band around 250 nm, which is intense only in the spectra of compounds **2** and **5**, a very intense band in the 263-281 nm region and two broad low intensity bands in the 333-350 nm region (shoulder) and in the visible region between 468 and 531 nm (Table 1).

The lowest energy band assigned to intramolecular charge transfer is the most influenced by the nature of the substituent, both on the nitrogen atom (CH$_3$ *vs*. H) and on the naphthoquinone ring (Cl *vs*. SR). Electron releasing
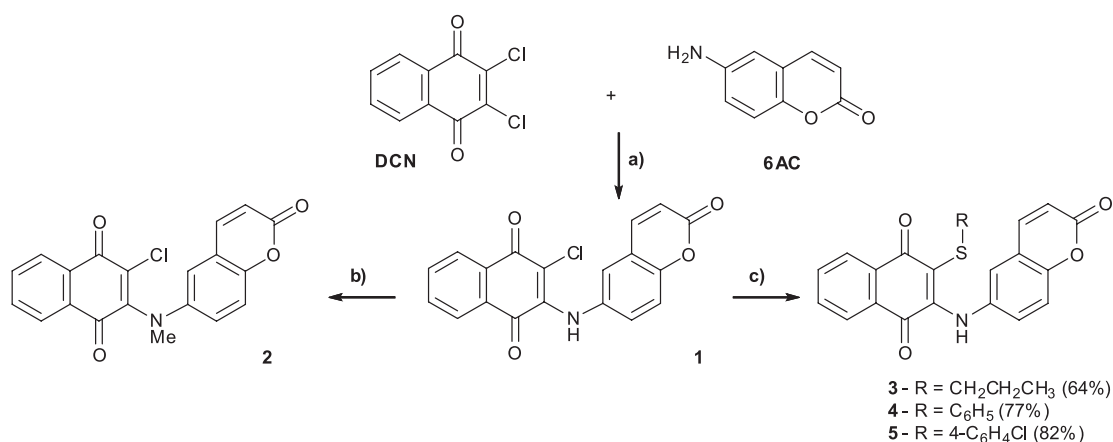
Scheme 1. The synthetic routes to compounds **1-3**. Reactions and conditions: a) DMF, 60-70 °C, 72 h; b) K$_2$CO$_3$/CH$_3$I, DMF, RT; c) thiol/Et$_3$N, DMF (**3**) or MeOH (**4**, **5**), 60-70 °C.
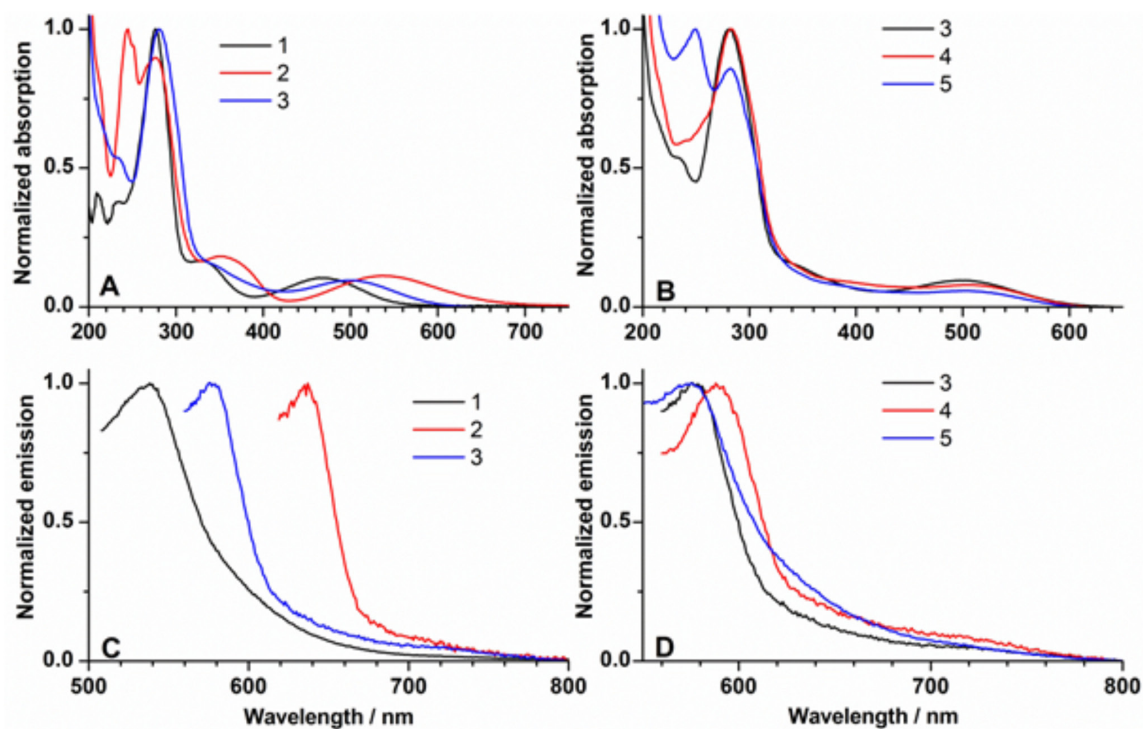
Figure 1. Normalized absorption (A and B) and emission (C and D) spectra of aminocoumarin-napthoquinone conjugates **1-5** in CH_3CN.

groups on the nitrogen (CH_3) and on the quinone ring (SR) shift this band to higher wavelengths. This red shift is more pronounced upon methylation of the nitrogen atom (**2** *vs.* **1**) than upon thiolation on the naphthoquinone ring (**3-5** *vs.* **1**). The spectra of the three thiolate compounds **3-5** are very similar, except for the high energy band, as expected.

Excitation of the lowest energy absorption band, $\lambda_{max}(3)$ of all compounds results in a very weak emission around 600 nm. Compound **1** has an emission maximum at 538 nm, between the values found for the 6-AC ($\lambda_{em} = 516$ nm) and 2-amino-3-chloro-1,4-naphthoquinone **6** ($\lambda_{em} = 592$ nm) emissions (Figure 2). Furthermore, the data gathered in Table 1 evidence that substitution of a hydrogen atom for a naphthoquinonyl group in 6-AC (compounds **1-5**) results in strong quenching of the aminocoumarin fluorescence

($\Phi = 0.25$)[23]. Approximately the same Stokes shift values are observed for all compounds suggesting that their excited state geometries are similar.[33]

Electrochemical properties

The electrochemical behavior of compounds **1**-**5** was investigated by cyclic voltammetry experiments which were carried out in argon-purged CH_3CN/Bu_4NClO_4, at 25 °C (see Figure 3 and Figures S19-S24 in the SI section). The cyclic voltammograms have been obtained in the potential range of –2.0 to +1.5 V *vs.* FcH/FcH[+] in four scan rates (50, 100, 250 and 500 mV). The reduction potentials, LUMO level, HOMO level and optical gap are given in Table 1. The LUMO level was determined using

Table 1. Optical properties, electrochemical data, calculated HOMO, LUMO and gap*opt* of compounds **1-5**

Compound	$\lambda_{max}(3)$ / nm	log ε_3	λ_{em} / nm	$\Delta\lambda$ / eV[a]	F	$E_{1/2}$ / mV[b] (ΔE_p / mV)			HOMO / eV[c]	LUMO / eV[d]	gap*opt* / eV[e]
						Wave I	Wave II	Wave III			
1	468	3.66	538	0.35	0.0001	–1000 (77)	–1374 (93)	–	–6.25	–3.80	2.45
2	538	3.59	637	0.36	0.0001	–905 (96)	–1320 (94)	878 (86)	–6.00	–3.90	2.10
3	495	3.54	575	0.34	0.0003	–1084 (74)	–1422 (100)	–	–5.98	–3.72	2.26
4	503	3.39	588	0.35	0.0003	–1045 (123)	–1420 (104)	–	–5.99	–3.76	2.24
5	499	3.15	574	0.32	0.0001	–1036 (102)	–1407 (95)	–	–5.99	–3.76	2.23

[a]Stokes shift; [b]data from voltammetric experiments in a cathodic scan, obtained at a scan rate of 100 mV s^{−1} in CH_3CN + 0.1 mol L^{−1} n-Bu_4NClO_4, at 25 °C; potential values are reported *vs.* ferrocene/ferrocenium (FcH/FcH[+]); [c]HOMO = LUMO*elec.* − gap*opt.*; [d]calculated from the reversible first reduction process (wave I); [e]optical gap estimated from the optical absorption edge. The inflection point in the first derivatives of the absorption spectrum was used.
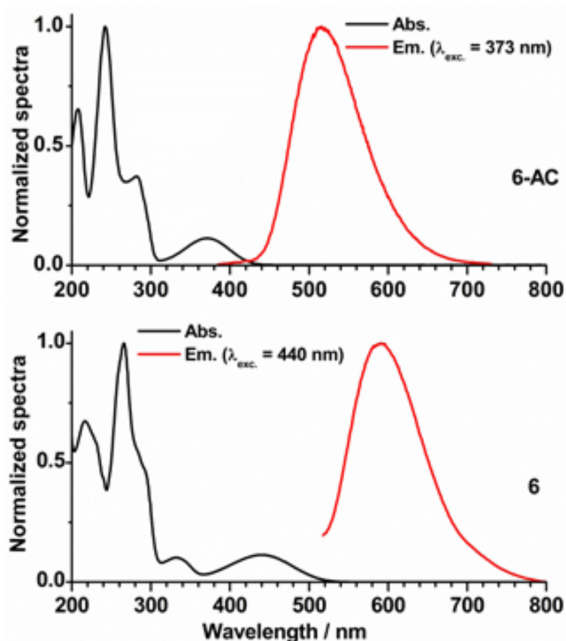
Figure 2. Normalized absorption and emission spectra of 6-AC and napthoquinone **6** in CH_3CN.

the equation $E_{LUMO} = -4.79 - E_{red}$ (wave I, *vs.* FcH/FcH$^+$).[34-39] The HOMO energy levels of all compounds were calculated by subtracting the optical gap. As observed for other 2-(R-phenyl)amine)-1,4-naphthoquinones[13] the voltammograms in CH_3CN show two successive one-electron reduction processes which generate two separate cathodic waves.

According to the data, both processes are *quasi* reversible (Figures S19-S24 in the SI section). The first process is attributed to the reduction of the quinone to
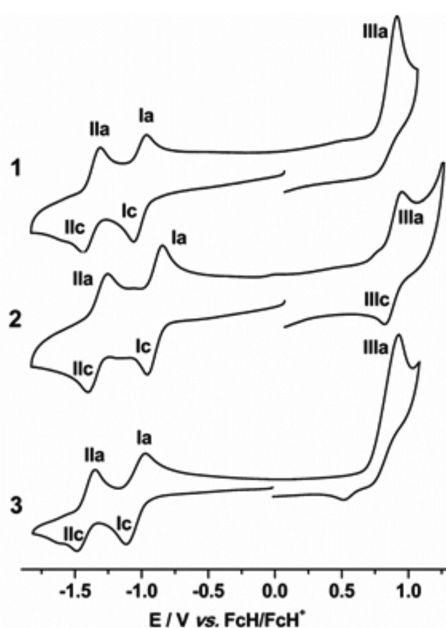

Figure 3. Cyclic voltammograms at 100 mV s^{-1} of **1**, **2** and **3**.
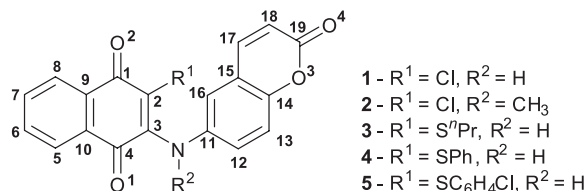
the semiquinone radical Q$^{•-}$ (Ic/Ia) and the second one is associated to the reduction of the semiquinone to the quinone dianion (IIc/IIa), Q^{2-}. Substitution of the chloro electron attracting group on the naphthoquinone ring in **1** for thiolate groups in **3-5** produces a sizeable cathodic shift for the two one-electron reduction processes, i.e., the presence of these electron donor groups makes the reduction of compounds **3-5** more difficult than reduction of **1**. The magnitude of the observed cathodic shift with respect to that of **1** for the first wave is roughly equal to 84 (**3**), 45 (**4**) and 36 (**5**) mV at 100 mV s^{-1}. The presence of the methyl group bonded to the nitrogen atom in **2** produces an anodic shift for the two one-electron steps of about 95 (wave I) and 50 mV (wave II), i.e., naphthoquinone **2** is more easily reduced than **1**, possibly due to the structural changes caused by the presence of the methyl group (see discussion below). Furthermore, the oxidation process (IIIa) at positive potential observed in the voltammograms of compounds **1** and **3-5** associated to the aminocoumarin nucleus is *quasi* reversible in the voltammogram of compound **2**. Thus, the methyl group on the nitrogen atom makes the oxidation product of **2** more stable than the oxidation products of the other compounds containing the NH group, which can undergo a number of side reactions.[40] No correlation is observed between the nature of the substituent and the oxidation process IIIa in the CVs of compounds **1** and **3-5** (see Figures S19-S24 in the SI section).

Theoretical calculations

In order to understand the spectroscopic and electrochemical properties of the aminocoumarin-naphthoquinone conjugates **1-5** calculations were carried out using DFT at the B3LYP/6-31+G(d,p) level (see Tables S1-S4 in the SI section).[41,42] The geometry of compound **1** was fully optimized starting from the CIF file obtained from the X-ray diffraction experiment.[32] The geometries of the other compounds were based on this structure. To evaluate the individual contributions of the molecules that represent the fragments composing these conjugates, calculations of 6-AC and 2-amino-3-chloro-1,4-naphthoquinone **6** were also carried out.

Geometries of the ground (S$_0$) and excited (S$_1$) state structures: The ground state (S$_0$) structures of compounds **1** and **3-5** (see Table 2 for the numbering of the atoms and values of selected structural parameters) contain a N1–H...O1 intramolecular electrostatic interaction.[32] They exhibit similar C3–N1–C11 angles, however small changes are noted in the values of the dihedral C2–C3–N1–C11 and C16–C11–N1–C3 angles as a function of R^1. The presence

Table 2. Selected angles for compounds **1-5** [°] in the ground (S_0) and excited (S_1) states

1 - R^1 = Cl, R^2 = H
2 - R^1 = Cl, R^2 = CH_3
3 - R^1 = S^nPr, R^2 = H
4 - R^1 = SPh, R^2 = H
5 - R^1 = SC_6H_4Cl, R^2 = H

Compound	C2–C3–N1–C11		C16–C11–N1–C3		C3–N1–C11		β^a
	S_0	S_1	S_0	S_1	S_0	S_1	S_0
1(X-ray)[32]	31.9 (30.8)	92.8	31.2 (29.6)	3.0	130.5 (129.2)	125.6	10.0
2	52.2	91.0	26.6	1.8	122.6	121.3	1.5
3	36.3	99.2	30.4	4.9	129.2	125.7	12.8
4	32.8	100.4	36.4	4.7	129.5	125.7	11.5
5	32.8	99.0	37.2	4.0	129.5	125.7	11.2

^{a}Pyramidalization angle β of amine: angle between the N–H or N–CH_3 bond and the C3–N–C11 plane.

of the propylthiolate group in compound **3** leads to larger C2–C3–N1–C11 and smaller C16–C11–N1–C3 dihedral angles in comparison to compounds **4** and **5**.

Differently, compound **2** which contains a methyl group on N1 does not exhibit the N1–H…O1 intramolecular electrostatic interaction and therefore the C2–C3–N1–C11 dihedral angle is much larger in this molecule than in the other compounds (Table 2) with a consequent decrease in the C16–C11–N1–C3 dihedral angle. Furthermore, the C3–N1–C11 angle is smaller in **2** (122 °) than in compounds **1** and **3-5** (approximately 130 °). This may be associated to the larger degree of pyramidalization (β angle, see Table 2) on the nitrogen atom in the latter compounds compared to compound **2**, possibly due to the N1–H…O1 electrostatic interaction in **1** and **3-5**. In all cases short C3–N1 bond distances (1.361 – 1.391 Å, see Table S1 in the SI section) are observed, indicating in all cases partial double bond character and therefore conjugation between the two fragments.

The excited state (S_1) structures of compounds **1, 3-5** do not exhibit the electrostatic N1–H…O1 interaction present in the S_0 structures. Elongation of the C3–N1 bond distance in compound **1** in the S_1 structure (from 1.359 Å in the S_0 structure to 1.432 Å) and decrease of the C11–N1 bond distance (1.416 Å to 1.343 Å from S_0 to S_1, respectively, see Table S1 in the SI section) are noted. Same trend is observed for compounds **2, 3-5**. Importantly, analysis of the dihedral C2–C3–N1–C11 angles in all compounds (Table 2) reveals that in the S_1 structures the naphthoquinone and coumarin rings are practically perpendicular to each other, suggesting that the electronic transition is a twisted intramolecular charge transfer (TICT).[22]

The S_0 and S_1 structures of 6-AC and naphthoquinone **6** were also calculated and the differences are discussed in relation to those observed for compound **1**. A comparative analysis of the bond distances (see Tables S1-S4 in the SI section) in these structures confirms the conjugation of the two fragments (coumaryl and naphthoquinonyl) through the nitrogen heteroatom in **1** as discussed above, as well as the donor acceptor character (push-pull) of 6-AC.

Analysis of the Mulliken charges (see Tables S5 and S6 in the SI section) for compounds **1-4** shows that naphthoquinone oxygens O1 and O2 are more negative in the S_1 than in the S_0 structures whereas coumaryl oxygens O3 and O4 are less negative in the S_1 than in the S_0 structures, thus indicating that the naphthoquinone nucleus is a better electron acceptor than the coumaryl lactone.

Ground state molecular orbital analysis: The contour plots of the frontier orbitals (HOMOs and LUMOs) and their corresponding energy levels and gaps are shown in Figure 4. The HOMO of **1** is located over both moieties, mostly on the coumarin (except on C17 and C19, see figure in Table 2 for the numbering), and to a lesser extent on the quinone (on O2–C1–C2–C3–N1). A smaller contribution of the quinone fragment to the HOMO of **2** is observed in comparison with **1, 3-5**. Substitution of the Cl group in **1** for thiolate groups in **3-5** results in the participation of this group to the HOMO. The aromatic thiolate groups have a significant contribution to the HOMO of compounds **4** and **5**. The LUMOs of all compounds have higher amplitude on the quinone ring (e_{1g} type symmetry) with some contribution of the nitrogen atom.

The calculated ground state energy gaps (**2** < **3-5** < **1**) are compatible with the red shifts (gap_{opt}) observed in the absorption spectra (Table 2) on going from compound **1** to compound **2** and from compound **1** to compounds **3-5**.
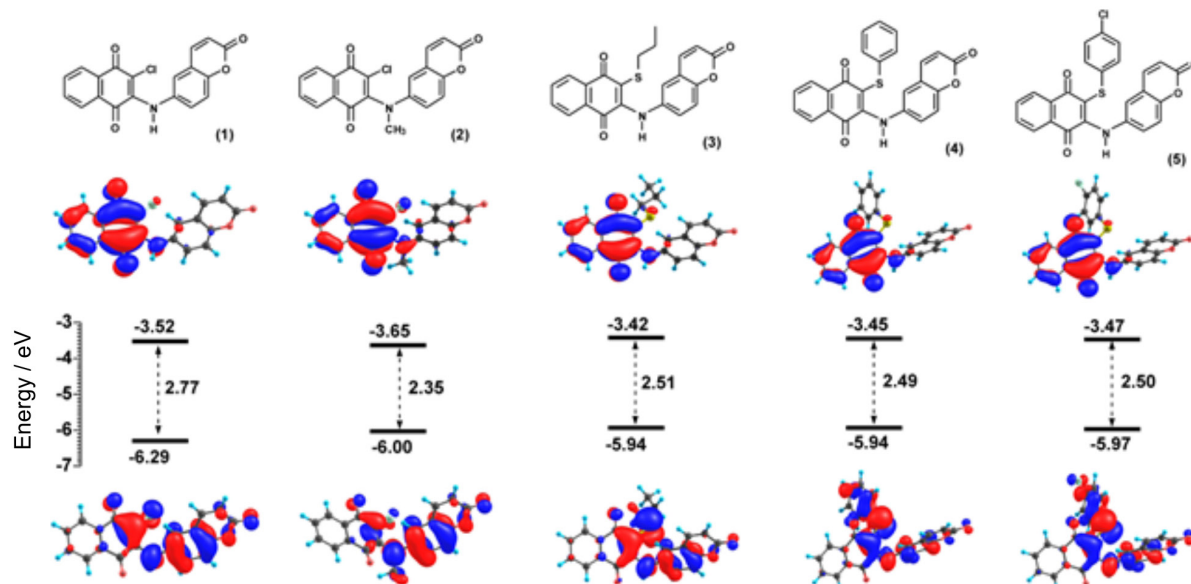
Figure 4. Frontier orbitals [contour values plotted at 0.03 (e/Bohr^3)$^{1/2}$] and energy diagrams for compounds **1**-**5**.

The LUMO energies of all compounds show a linear correlation with their first reduction process (see Table 1 and Figure 3). Compound **2** with the most negative theoretical LUMO (–3.65 eV) is also the most easily reduced ($E_{1/2}$ = –0.905 V), whereas compound **3**, with the least negative LUMO, is the hardest to reduce. Both the shape and energy of the LUMO confirm that the naphthoquinone nucleus is the reduction electroactive site of the conjugates **1**-**5**.

Finally, the contour plots of the frontier orbitals (HOMOs and LUMOs) and the corresponding energy levels and gaps of 6-AC and compounds **6** and **1** are gathered in Figure 5. These results show that the HOMO energy of **1** is halfway between the HOMO energies of 6-AC and **6**. However, the
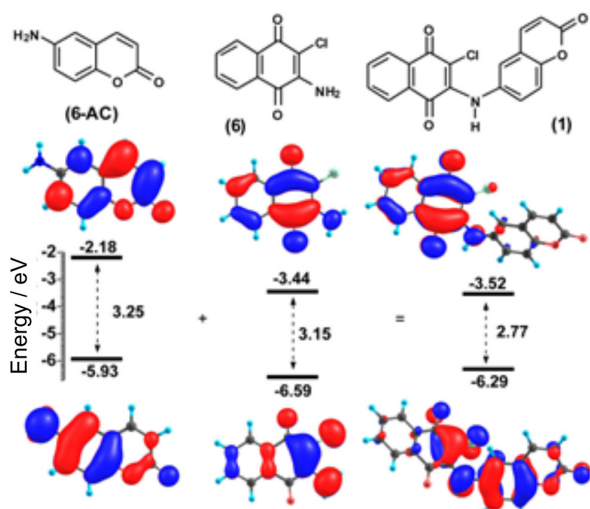
Figure 5. Molecular orbital diagrams for 6-AC, aminonaphthoquinone **6** and aminocoumarin-naphthoquinone conjugate **1** [contour values plotted at 0.03 (e/Bohr^3)$^{1/2}$].

LUMO of **6**, about 1.26 eV more stable than that of 6-AC, dominates both the LUMO shape and energy of **1**.

To assign the absorption bands observed in the UV-Vis spectra, the molecular orbitals of the compounds were calculated in CH$_3$CN using the PCM model. The theoretical absorption spectra (see Figures S25-S31 in the SI section) show a systematic underestimation of the excitation energies for 6-AC, **6** and **1**-**5** as previously observed for other systems.[43-47] The largest differences have been observed for the charge-transfer bands of the conjugates. In spite of this limitation, the important features of the spectra have been correctly simulated. The HOMO–LUMO transitions for all compounds are $\pi \rightarrow \pi^*$ in nature.

To understand the fluorescence quenching of the conjugates the frontier orbitals in the singlet excited state conformations (S$_1$) have been calculated and are displayed in Figure 6. The S$_1$ geometries of the molecules are very different from those in the S$_0$ state. The geometry change is related to the increase of the torsion angle between the naphthoquinone and aminocoumarin fragments (Table 2). As a consequence the HOMO is localized on the aminocoumarin and the LUMO on the naphthoquinone moiety in the excited state. It is evident from calculated HOMO-LUMO energies (Figure 6) that all 6-aminocoumarin-naphthoquinone conjugates behave as push-pull systems and that fluorescence quenching for all compounds may be related to the stronger π-electron acceptor character of the naphthoquinone compared to that of the coumaryl fragment. The naphthoquinone LUMO is of lower energy than that of 6-AC (see Figure S35 in the SI section) in both the ground and excited states. Thus the energy states are such that the fluorescent group (6-AC)
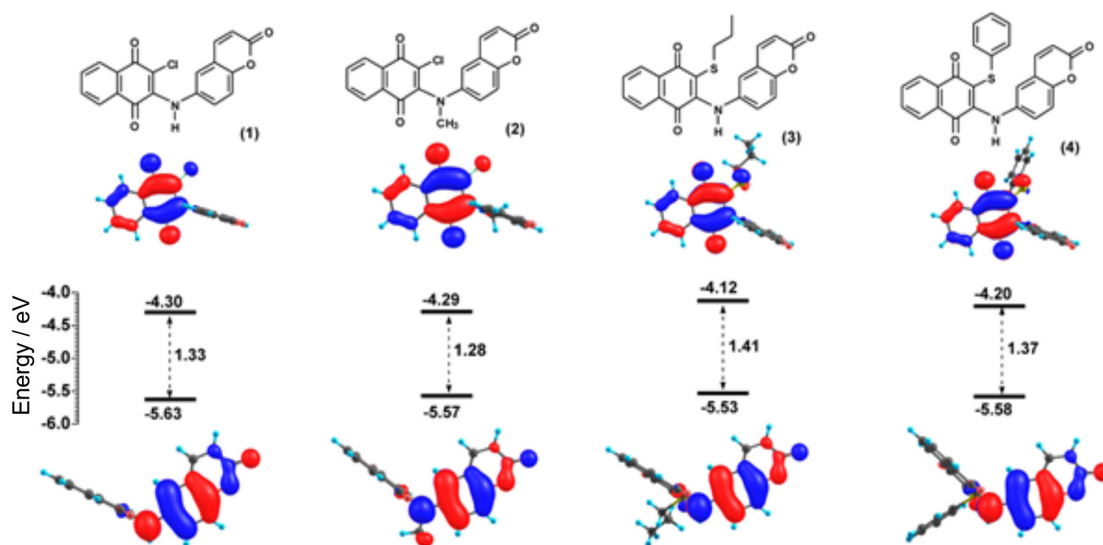
Figure 6. Frontier orbitals in the excited state conformations (S$_1$) [contour values plotted at 0.03 (e/Bohr^3)$^{1/2}$] and energy diagrams for compounds **1**-**5**.

donates electrons to the naphthoquinone LUMO resulting in an oxidative photoinduced electron transfer (oxidative-PET).[48]

Conclusions

In this study the fluorescent dye 6-AC was attached to 1,4-naphthoquinone derivatives aiming at fluorescent molecules. However the fluorescence of 6-AC was quenched in the 6-aminocoumarin-naphthoquinone conjugates **1**-**5**. To explain these results, experimental and theoretical investigations of the photophysical and electrochemical properties of conjugates **1**-**5**, 6-AC and 2-amino-3-chloro-1,4-naphthoquinone **6** were carried out in CH$_3$CN. The strong π-electron acceptor character of the naphthoquinone moieties was confirmed by electrochemical measurements which showed a reduction potential around −1.0 V. Substitution on either N (H for CH$_3$) or on the quinone ring (Cl for thiols) did not result in significant changes (wave I, Δ = ± 0.1 V) on the electrochemical properties of the conjugates. TD-DFT calculations including solvent effects using the PCM model revealed that the S$_0$ structures of compounds **1**, **3**-**5** exhibit an intramolecular electrostatic N1–H...O1 interaction which does not exist in the S$_1$ structures. An analysis of the S$_1$ structures suggests that the electronic transition is a twisted intramolecular charge transfer (TICT). The lowest energy absorption band in the spectra of all conjugates has been assigned to π–π* charge transfer from aminocumaryl to naphthoquinone. The emission of all conjugates significantly decreased (Φ = 10^{-4}) compared to 6-AC (Φ = 0.25). This observation has been explained in terms of the strong electron acceptor nature of the naphthoquinone moiety and conjugation of

the two moieties through the imine like nitrogen which allow the oxidative-PET. It was found that the LUMO orbital is located on the naphthoquinone and controls both electrochemical and photophysical properties of all conjugates. It would therefore be interesting, in future studies, to introduce a saturated spacer to avoid quenching of the coumarin fluorescence.

Experimental section

Materials and instruments

All starting materials were used without previous treatment and solvents, as received from commercial suppliers (except for triethylamine and *N,N*-dimethylformamide, which were previously distilled). Thin-layer chromatography (TLC) was performed on aluminum sheets coated with silica gel 60F-254 (Sorbent). The plates were inspected by UV light (λ = 254 nm). Silica gel 60 Merck (0.063-0.200 mm) was used for column chromatography. 6-Aminocumarin was synthesized according to the literature.[49]

^{1}H NMR and ^{13}C NMR spectra were recorded on a Varian Unit Plus (300 MHz or 500 MHz) spectrometer in CD$_3$Cl, CD$_3$CN or DMSO-d$_6$. Chemical shifts (δ) are reported in parts per million (ppm) relative to the signal of residual solvent. The hydrogen signals were attributed through coupling constant values and ^{1}H × ^{1}H – COSY experiments. Elemental analyses were performed using a Perkin-Elmer CHN 2400 microanalyzer (Central Analítica - Instituto de Química, Universidade de São Paulo, Brazil). Melting points were obtained on a Digital Melting Point IA9100 (ThermoFisher Scientific-USA) and are

uncorrected. Transmission infrared spectra were recorded on an FT-IR Varian 660 spectrophotometer, equipped with a Pike ATR Miracle accessory (diamond/ZnSe crystal, resolution: 4 cm⁻¹). Cyclic voltammograms were obtained with a BAS Epsilon potentiostat-galvanostat system at room temperature, using n-Bu$_4$NClO$_4$ (0.1 mol L⁻¹) as the supporting electrolyte in CH$_3$CN (spectroscopic grade) solutions of the compounds (at 1.0 × 10⁻³ mol L⁻¹). The electrochemical cell was a conventional one with three electrodes: Ag/Ag⁺ was used as the quasi reference electrode, a platinum wire as the auxiliary electrode and glassy carbon as the working electrode. The ferrocene/ferrocenium (FcH/FcH⁺) couple was added at the end of each experiment as internal standard to the bulk solution; the data are thus reported versus the FcH/FcH⁺ couple as recommended by IUPAC.[50] Pure argon was bubbled through the electrolytic solution to remove oxygen in all experiments. UV-vis absorption spectra were recorded on a Cary 50 (Varian) spectrophotometer using spectroscopic grade CH$_3$CN. The values of wavelength are expressed in nanometers (nm) and epsilons (ε) in their logarithmic form. Luminescence spectra were obtained in a Varian Cary Eclipse fluorescence spectrophotometer. Fluorescence quantum yields were determined using a quinine sulfate (QB) solution in 0.5 mol L⁻¹ H$_2$SO$_4$ (Φ = 0.546)[51] as reference. The quantum yield was determined using the following equation: [52]

$$\Phi_{em,S} = \Phi_{em,R}(f_R/f_S)(I_S/I_R)(n_S/n_R) \tag{1}$$

where $\Phi_{em,}s$ represents the fluorescence quantum yield of the sample; f_S and f_R are the absorption factor ($f = 1 - 10^{-Abs}$, where Abs = absorbance) for the sample and the reference, respectively, at the excitation wavelength; I_S and I_R denote the integrated areas of the corrected emission spectra for the sample and the reference, respectively; and n_S and n_R are the refractive indices of the sample and reference solvents, respectively.

Calculations

DFT calculations were performed with the Gaussian 09 (Rev. B.01) software package.[53] The geometry of compound **1** was fully optimized using the geometry obtained in the solid state measurements.[32] Compounds **2-5** did not provide single crystal and their geometry optimizations were carried out based on the geometry of compound **1**. For the geometry optimization calculation the B3LYP functional together with the 6-31+G(d,p) basis set was employed.[54,55] Harmonic frequency calculations were performed for the optimized geometries and revealed

that these geometries represent genuine minimum energy points (with no negative eigenvalue) on the potential energy surface. Based on the B3LYP/6-31+G(d,p) optimized geometries, TD-DFT approaches were used to calculate vertical excitations with linear responses to verify the effects of these excitations on the absorption spectra of the examined compounds. The polarized continuum (overlapping spheres) solvation model (PCM) was used to ensure that solvent effects (CH$_3$CN) were incorporated into all of the aforementioned calculations. The PCM computations used the UFF radii and all of the standard specifications of the Gaussian package. The TD results were analysed with the GaussSum 2.2 software.[56] The absorption spectra were fitted with a Gaussian function with a FWHM of 3000 cm⁻¹.

Synthesis

2-chloro-3-(2-oxo-2H-chromen-6-ylamino)naphthalene-1,4-dione **1**: described elsewhere, see Supplementary Information.[32]

2-chloro-3-(methyl(2-oxo-2H-chromen-6-yl)amino) naphthalene-1,4-dione **2**: N-methylation of compound **1** was carried out as previously described for other 2-(R-phenyl) amino-1,4-naphthoquinones,[31] from 351.7 mg, 1 mmol of **1**. After reaction completion the volatiles were removed under reduced pressure. The crude product was purified by column chromatography on silica gel (eluent CH$_2$Cl$_2$), giving a purple solid. Yield: 237.8 mg, 65%; m.p. 196 °C; calcd. for C$_{20}$H$_{12}$ClNO$_4$: C, 65.67; H, 3.31; N, 3.83%; found: C, 65.01; H, 3.43; N, 3.79%; ¹H NMR (DMSO-d$_6$, 500 MHz): δ 8.10 (d, 1H, J 6.8 Hz), 8.00 (d, 1H, J 6.8 Hz), 7.93 (d, 1H, J 9.6 Hz), 7.91-7.87 (m, 2H), 7.32 (t, 1H, J 1.6 Hz), 7.26 (d, 2H, J 1.6 Hz), 6.45 (d, 1H, J 9.6 Hz), 3.38 (s, 3H); ¹³C NMR-APT (DMSO-d$_6$, 75 MHz): δ 180.44, 178.06, 160.67, 149.10, 148.28, 143.28, 143.05, 136.13, 134.41, 134.16, 131.50, 131.44, 127.39, 127.16, 121.83, 119.29, 117.62, 117.42, 114.78, 39.95; IR (KBr; ν$_{max}$/cm⁻¹): 3080 (C–H$_{arom.}$), 2923 (C–H$_{aliph.}$), 1718 (C=O$_{ester}$), 1677 (C=O$_{quin.}$), 1639 (C=O$_{quin.}$), 1543 (C=C); UV-Vis [CH$_3$CN; λ$_{max}$/nm (log ε)]: 263 (4.72), 350 (3.94), 536 (3.59).

2-(2-oxo-2H-chromen-6-ylamino)-3-(propylthio) naphthalene-1,4-dione **3**: 1-Propanethiol (87 µL, 0.96 mmol) was added to a solution of **1** (170 mg, 0.48 mmol) in DMF (20 mL) in the presence of triethylamine (66.4 µL, 0.48 mmol). The mixture was stirred at 60-70°C for 24 h. After removal of the solvents under reduced pressure, the crude product was purified through recrystallization in cyclohexane, resulting in a purple solid. Yield: 25.3 mg,

64%; m.p. 134 °C; calcd. for $C_{22}H_{17}NO_4S$: C, 67.50; H, 4.38; N, 3.58%; found: C, 67.69; H, 4.51; N, 3.45%; ^{1}H NMR (500 MHz, CD_3CN): δ 8.12 (t, 2H, *J* 7.7 Hz), 7.88-7.83 (m, 2H), 7.79 (dt, 1H, *J* 7.7, 1.3 Hz), 7.39 (dd, 2H, *J* 8.8, 2.5 Hz), 7.34 (d, 1H, *J* 8.8 Hz), 7.32 (d, 1H, *J* 2.5 Hz), 6.45 (d, 1H, *J* 9.6 Hz), 2.58 (t, 2H, *J* 7.2 Hz), 1.44-1.35 (m, 2H), 0.84 (t, 3H, *J* 7.2 Hz); ^{13}C NMR-APT ($CDCl_3$, 75 MHz): δ 180.8, 180.0, 160.4, 150.7, 144.5, 142.8, 134.7, 134.6, 133.2, 132.8, 130.3, 126.8, 126.6, 126.0, 120.4, 118.7, 118.3, 117.3, 116.9, 45.7, 35.8, 8.50; IR (KBr; $ν_{max}/cm^{-1}$): 3329 (N–H), 3079 ($C–H_{arom.}$), 2957 ($C–H_{aliph.}$), 1721 ($C=O_{ester}$), 1658 ($C=O_{quin.}$), 1639 ($C=O_{quin.}$), 1560 (C=C); UV-Vis [CH_3CN; $λ_{max}/nm$ (log ε)]: 281 (4.56), 348 (3.73), 500 (3.54).

3-(2-oxo-2H-chromen-6-ylamino)-3-(arythiol) naphthalene-1,4-dione 4 and (2-oxo-2H-chromen-6-ylamino)-3-(4-chloroarythiol) naphthalene-1,4-dione 5: Compounds **4** and **5** were synthesized as described in the literature[28] for analogous compounds 351 mg (1 mmol) of **1** and 1 mmol of the respective aryl thiols in absolute MeOH (20 mL), under reflux, in the presence of triethylamine (2.5 mmol). After 8 h, the resulting solution was concentrated under vacuum and purified by column chromatography on silica gel using EtOAc/hexane. **4**: yield: 317 mg, 77%; m.p. 240 °C; calcd. for $C_{24}H_{15}NO_4S$: C, 69.72; H, 3.66; N, 3.39%.; found: C, 67.88; H, 3.52; N, 3.30%; ^{1}H NMR (DMSO-d_6, 500 MHz): δ 8.20 (d, 1H, *J* 7.6 Hz), 8.13 (d, 1H, *J* 7.6 Hz), 7.99 (t, 1H, *J* 7.4 Hz), 7.95 (d, 1H, *J* 7.4 Hz), 7.91 (d, 1H, *J* 9.5 Hz), 7.25-7.23 (m, 1H), 7.19-7.16 (m, 5H), 6.86 (d, 1H, *J* 7.3 Hz), 6.85 (d, 1H, *J* 5.9 Hz), 6.54 (d, 1H, *J* 9.5 Hz); IR (KBr; $ν_{max}/cm^{-1}$): 3306 (N–H), 3080 ($C–H_{arom.}$), 1733 ($C=O_{ester}$), 1678 ($C=O_{quin.}$), 1664 ($C=O_{quin.}$), 1551 (C=C); UV-Vis [CH_3CN; $λ_{max}/nm$ (log ε)]: 284 (4.47), 505 (3.39). **5**: yield: 365 mg, 82%; m.p. 210 °C; calcd. for $C_{24}H_{14}ClNO_4S$: C, 64.36; H, 3.15; N, 3.13%.; found: C, 62.58; H, 3.24; N, 3.03%; ^{1}H NMR (DMSO-d_6, 500 MHz): δ 8.20 (d, 1H, *J* 7.6 Hz), 8.13 (d, 1H, *J* 7.6 Hz), 7.99 (t, 1H, *J* 7.4 Hz), 7.96-7.92 (m, 2H), 7.26 (d, 1H, *J* 9.5 Hz), 7.22-7.19 (m, 4H), 6.88 (d, 2H, *J* 8.6 Hz), 6.56 (d, 1H, *J* 9.5 Hz); IR (KBr; $ν_{max}/cm^{-1}$): 3267 (N–H), 3079 ($C–H_{arom.}$), 1742 ($C=O_{ester}$), 1663 ($C=O_{quin.}$), 1627 ($C=O_{quin.}$), 1537 (C=C); UV-Vis [CH_3CN; $λ_{max}/nm$ (log ε)]: 282 (4.29), 510 (3.15).

Supplementary information

Supplementary Information associated with the paper contains FTIR, ^{1}H, ^{13}C NMR spectra, cyclic voltammograms of the compounds and computational details. These data are available free of charge at http://jbcs.sbq.org.br as a PDF file.

References

1. Hallak, M.; Win, T.; Shpilberg, O.; Bittner, S.; Granot, Y.; Levy, I.; Nathan, I.; *Brit. J. Haematol.* **2009**, *147*, 459.

2. Esteves-Souza, A.; Figueiredo, D. V.; Esteves, A.; Camara, C. A.; Vargas, M. D.; Pinto, A. C.; *Braz. J. Med. Biol. Res.* **2007**, *40*, 1399.

3. Esteves-Souza, A.; Lúcio, K. A.; Cunha, A. S.; Pinto, A. C.; Lima, E. L. S.; Camara, C. A.; Vargas, M. D.; Gattass, C. R.; *Onc. Rep.* **2008**, *20*, 225.

4. Francisco, A. I.; Casellato, A.; Neves, A. P.; Carneiro, J. W. D; Vargas, M. D.; Visentin, L. C.; Magalhães, A.; Camara, C. A.; Pessoa, C; Costa-Lotufo, L. V.; Marinho, J. D. B.; Moraes, M. O.; *J. Braz. Chem. Soc.* **2010**, *21*, 169.

5. Barbosa, T. P.; Camara, C. A.; Silva, T. M. S.; Martins, R. M.; Pinto, A. C.; Vargas, M. D.; *Bioorg. Med. Chem.* **2005**, *13*, 6464.

6. Silva, T. M. S.; Camara, C. A.; Barbosa, T. P.; Soares, A. Z.; Cunha, L. C.; Pinto, A. C.; Vargas, M. D.; *Bioorg. Med. Chem.* **2005**, *13*, 193.

7. Kapadia, G. J.; Azuine, M. A.; Balasubramanian, V.; Sridhar, R.; *Pharmacol. Res.* **2001**, *43*, 363.

8. Ryu, C.-K.; Kim, D.-H.; *Arch. Pharm. Res.* **1992**, *15*, 263.

9. Clark, N. G.; *Pest. Sci.* **1985**, *16*, 23.

10. Koura, S.; Takasuka, K.; Katsuyama, N.; Ogino, C.; Sato, Y.; Wakabayashi, K.; *Biosc. Biotech. Biochem.* **1994**, *58*, 1210.

11. Silveira, G. Q.; Ronconi, C. M.; Vargas, M. D.; San Gil, R. A. S.; Magalhães, A.; *J. Braz. Chem. Soc.* **2011**, *22*, 961.

12. Glezer, V.; Stradins, J.; Friemanis, J.; Baider, L.; *Electrochim. Acta* **1983**, *28*, 87.

13. Aguilar-Martínez, M.; Cuevas, G.; Jiménez-Estrada, M.; González, I.; Lotina-Hennsen, B.; Macías-Ruvalcaba, N.; *J. Org. Chem.* **1999**, *64*, 3684.

14. Koyama, J.; Morita, I.; Kobayashi, N.; Osakai, T.; Hotta, H.; Takayasu, J.; Nishino, H.; Tokuda, H.; *Cancer Lett.* **2003**, *201*, 25.

15. Brun, M. P.; Braud, E.; Angotti, D.; Mondésert, O.; Quaranta, M.; Montes, M.; Miteva, M.; Gres, N.; Ducommun, B.; Garbay, C.; *Bioorg. Med. Chem.* **2005**, *13*, 4871.

16. Katritzky, A. R.; Narindoshvili, T.; *Org. Biomol. Chem.* **2009**, *7*, 627.

17. Krueger, A. T.; Imperiali, B.; *Chembiochem.* **2013**, *14*, 788.

18. Wang, F.; Tan, W. B.; Zhang, Y.; Fan, X.; Wang, M.; *Nanotechnology* **2006**, *17*, R1.

19. Silveira, G. Q.; Vargas, M. D.; Ronconi, C. M.; *J. Chem. Mater.* **2011**, *11*, 6034.

20. Johnson, I. D. In *Handbook of Biological Confocal Microscopy*, 3rd ed.; Pawley, J., ed.; Springer: New York, 2006.

21. Riveiro, M. E.; De Kimpe, N.; Moglioni, A.; Vazquez, R.; Monczor, F.; Shayo, C.; Davio, C.; *Curr. Med. Chem.* **2010**, *17*, 1325.

22. Krystkowiak, E.; Dobek, K.; Maciejewski, A.; *Photochem. Photobiol. Sci.* **2013**, *12*, 446.

23. Krystkowiak, E.; Dobek, K.; Burdzińskib, G.; Maciejewski, A.; *Photochem. Photobiol. Sci.* **2012**, *11*, 1322.

24. Rózsa, Z.; Mester, I.; Reisch, R.; Szendrei, K.; *Planta Med.* **1989**, *55*, 68.

25. Ito, C.; Ono, T.; Tanaka, E.; Takemura, Y.; Nakata, T.; Uchida, H.; Ju-ichi, M.; Omura, M.; Furukawa, H.; *Chem. Pharm. Bull.* **1993**, *41*, 205.

26. Ishikawa, T.; Kotake, K.; Ishii, H.; *Chem. Pharm. Bull.* **1995**, *43*, 1039.

27. Ibis, C.; Deniz, N. G.; *J. Chem. Sci.* **2012**, *124*, 657.

28. Tandon, V. K.; Maurya, H. T.; Mishra, N. N.; Shukla, P. K.; *Eur. J. Med. Chem.* **2009**, *44*, 3130.

29. Tandon, V. K.; Maurya, H. T.; Tripathi, A.; ShivaKeshava, G. B.; Shukla, P. K.; Srivastava, P.; Panda, D.; *Eur. J. Med. Chem.* **2009**, *44*, 1086.

30. Valente, C.; Moreira, R.; Guedes, R. C.; Iley, J.; Jaffarc, M.; Douglas, K. T.; *Bioorg. Med. Chem.* **2007**, *15*, 5340.

31. Lisboa, C. S.; Santos, V. G.; Vaz, B. G.; Lucas, N. C.; Eberlin, M. N.; Garden, S. J.; *J. Org. Chem.* **2011**, *6*, 5264.

32. Sousa, M. O. B.; Silveira, G. Q.; Gomez, J. A. G.; *Acta Cryst.* **2013**, *E69*, o1317.

33. Anslyn, E. V.; Dougherty, D. A.; *Modern Physical Organic Chemistry*; University Science Books: Sausalito, CA, 2006.

34. Liu, Y.; Liu, M. S.; Jen, A. K. -Y.; *Acta Polym.* **1999**, *50*, 105.

35. Chang, S. C.; Weaver, M. J.; *J. Phys. Chem.* **1991**, *95*, 5391.

36. Stuve, E. M.; Krasnopoler, A.; Sauer, D. E.; *Surf. Sci.* **1995**, *335*, 177.

37. Miller, L. L.; Nordbloman, G. D.; Maybda, E. A.; *J. Org. Chem.* **1972**, *37*, 916.

38. Pösch, P.; Thelakkat, M.; Schmidt, H. W.; *Synth. Met.* **1999**, *102*, 1110.

39. Pommerehne, J.; Vestweber, H.; Guss, W.; Mahrt, R. F.; Bassler, H.; Porsch, M.; Daub, J.; *Adv. Mater.* **1995**, *7*, 551.

40. Turovska, M.; Stradins, J.; Freimanis, J.; Strazdins, I.; Logins, J.; Dregeris, J.; *J. Electroanal. Chem.* **1996**, *414*, 221.

41. Becke, A. D.; *J. Chem. Phys.* **1993**, *98*, 5648.

42. Ditchfield, R.; Hehre, W. J.; Pople, J. A.; *J. Chem. Phys.* **1971**, *54*, 724.

43. Matos, C. R. M. O.; Miranda, F. S.; Carneiro, J. W. de M.; Pinheiro, C. B.; Ronconi, C. M.; *Phys. Chem. Chem. Phys.* **2013**, *15*, 13013.

44. Grimme, S.; Parac, M.; *ChemPhysChem* **2003**, *4*, 292.

45. Drew, A.; Head-Gordon, M. J.; *Am. Chem. Soc.* **2004**, *126*, 4007.

46. Tozer, D. J.; Handy, N. C.; *Phys. Chem. Chem. Phys.* **2000**, *2*, 2117.

47. Pastore, M.; Fantacci, S.; De Angelis, F. J.; *Phys. Chem. C* **2013**, *117*, 3685.

48. Loudet, A.; Burgess, K.; *Chem. Rev.* **2007**, *107*, 4891.

49. Morgan, G. T.; Gore, F. M.; *J. Chem. Soc. Trans.* **1904**, *85*, 1230.

50. Gritzner, G.; Kuta, J.; *Pure Appl. Chem.* **1984**, *56*, 461.

51. Adams, M. J.; Highfield, J. G.; Kirkbright, G. F.; *Anal. Chem.* **1977**, *49*, 1850.

52. Birks, J. B.; *Photophysics of Aromatic Molecules*, 1st ed.; Wiley-Interscience: London, 1970.

53. Gaussian 09, Revision B.01, Frisch, M. J.; Trucks, G. W.; Schlegel, H. B.; Scuseria, G. E.; Robb, M. A.; Cheeseman, J. R.; Scalmani, G.; Barone, V.; Mennucci, B.; Petersson, G. A.; Nakatsuji, H.; Caricato, M.; Li, X.; Hratchian, H. P.; Izmaylov, A. F.; Bloino, J.; Zheng, G.; Sonnenberg, J. L.; Hada, M.; Ehara, M.; Toyota, K.; Fukuda, R.; Hasegawa, J.; Ishida, M.; Nakajima, T.; Honda, Y.; Kitao, O.; Nakai, H.; Vreven, T.; Montgomery Jr., J. A.; Peralta, J. E.; Ogliaro, F.; Bearpark, M.; Heyd, J. J.; Brothers, E.; Kudin, K. N.; Staroverov, V. N.; Kobayashi, R.; Normand, J.; Raghavachari, K.; Rendell, A.; Burant, J. C.; Iyengar, S. S.; Tomasi, J.; Cossi, M.; Rega, N.; Millam, J. M.; Klene, M.; Knox, J. E.; Cross, J. B.; Bakken, V.; Adamo, C.; Jaramillo, J.; Gomperts, R.; Stratmann, R. E.; Yazyev, O.; Austin, A. J.; Cammi, R.; Pomelli, C.; Ochterski, J. W.; Martin, R. L.; Morokuma, K.; Zakrzewski, V. G.; Voth, G. A.; Salvador, P.; Dannenberg, J. J.; Dapprich, S.; Daniels, A. D.; Farkas, Ö.; Foresman, J. B.; Ortiz, J. V.; Cioslowski J.; Fox, D. J. Gaussian, Inc., Wallingford CT, 2009.

54. Becke, A. D.; *J. Chem. Phys.* **1993**, *98*, 5648.

55. Ditchfield, R.; Hehre, W. J.; Pople, J. A.; *J. Chem. Phys.* **1971**, *54*, 724.

56. O'Boyle, N. M.; Tenderholt; A. L.; Langner, K. M.; *J. Comp. Chem.* **2008**, *29*, 839.

Supplementary Information

6-Aminocoumarin-Naphthoquinone Conjugates: Design, Synthesis, Photophysical and Electrochemical Properties and DFT Calculations

Fabio S. Miranda, Célia M. Ronconi, Mikaelly O. B. Sousa,
Gleiciani Q. Silveira and Maria D. Vargas**

*Instituto de Química, Universidade Federal Fluminense,
Campus do Valonguinho, Centro, 24020-141 Niterói-RJ, Brazil*

1. FTIR and ¹H, ¹³C and NMR spectra

1.1. 2-chloro-3-(2-oxo-2H-chromen-6-ylamino)naphthalene-1,4-dione **1**
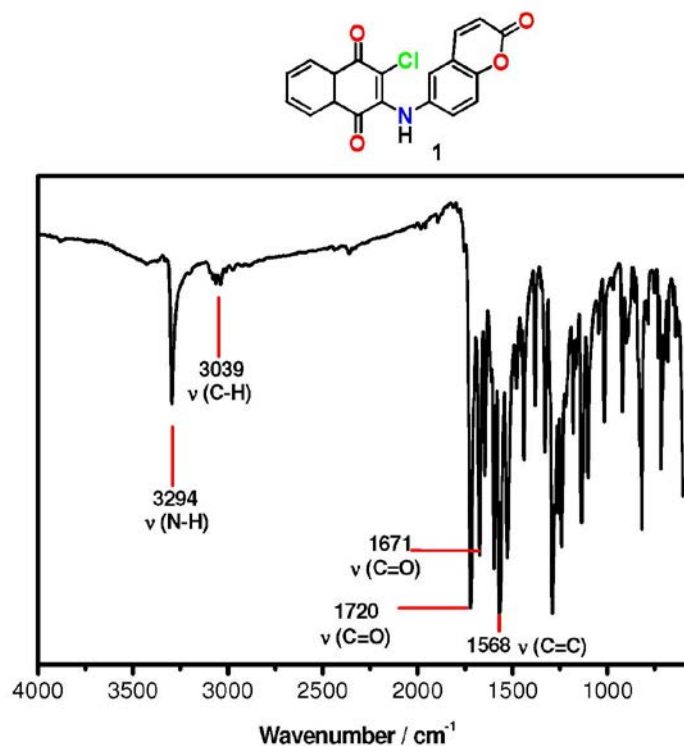
Figure S1. FTIR spectrum of compound **1** (KBr).

*e-mail: miranda@vm.uff.br, mdvargascp@gmail.com
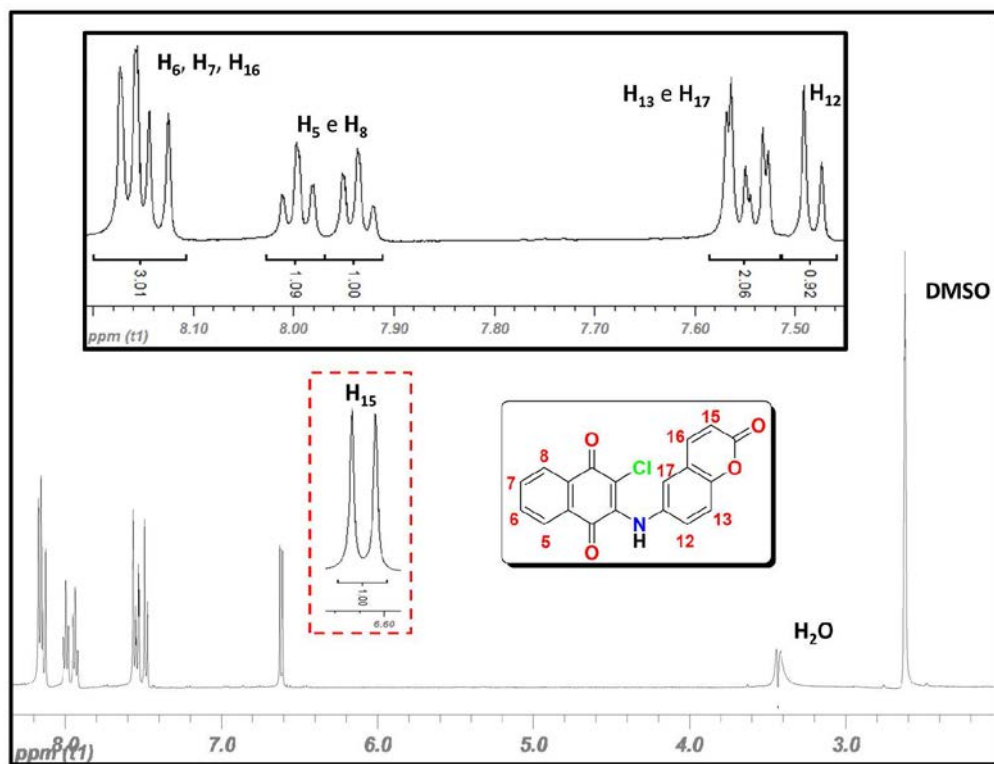
Figure S2. ¹H NMR spectrum of **1** in DMSO-d₆ (500 MHz).
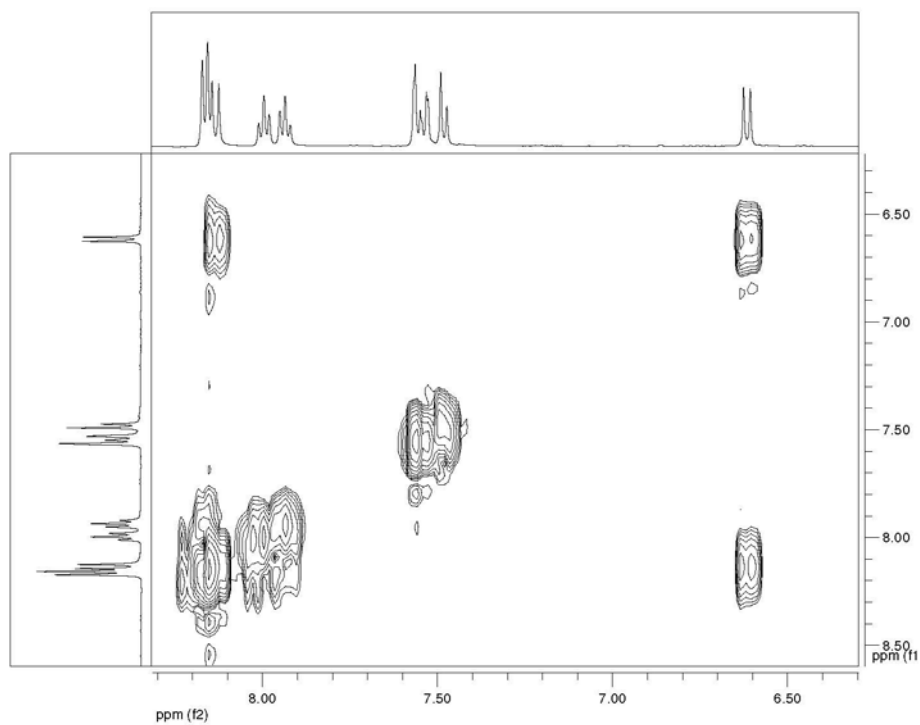
Figure S3. ¹H × ¹H – COSY of **1** in DMSO-d₆ (500 MHz).
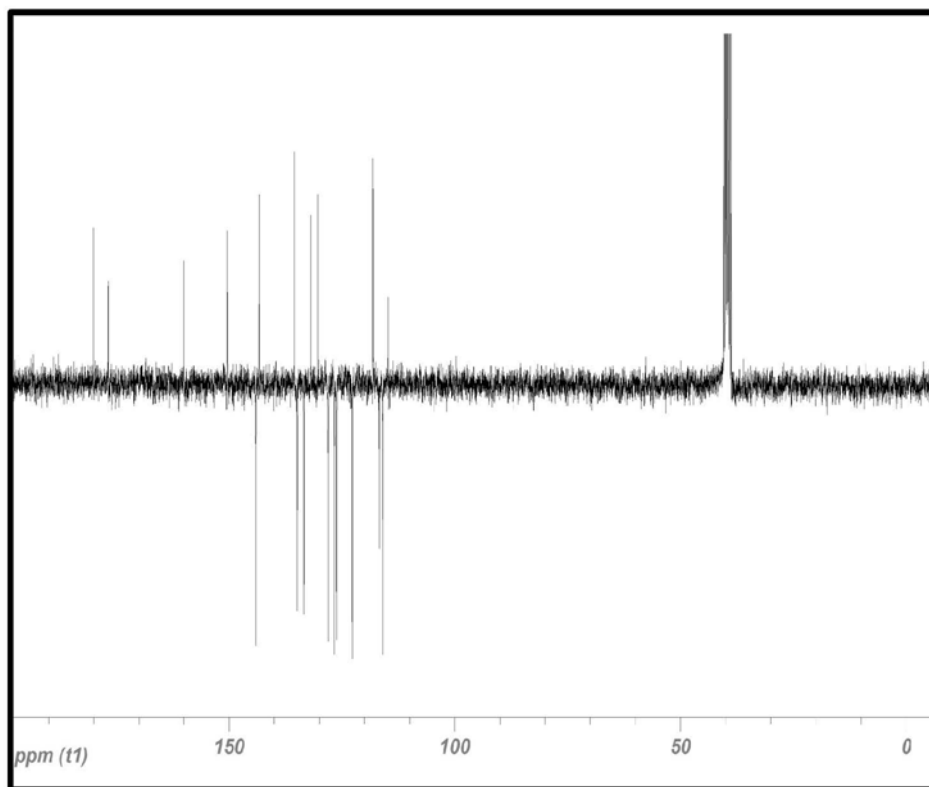
Figure S4. ^{13}C NMR-APT spectrum of **1** in DMSO-d$_6$ (75 MHz).

1.2. 2-chloro-3-(methyl(2-oxo-2H-chromen-6-yl)amino)naphthalene-1,4-dione **2**
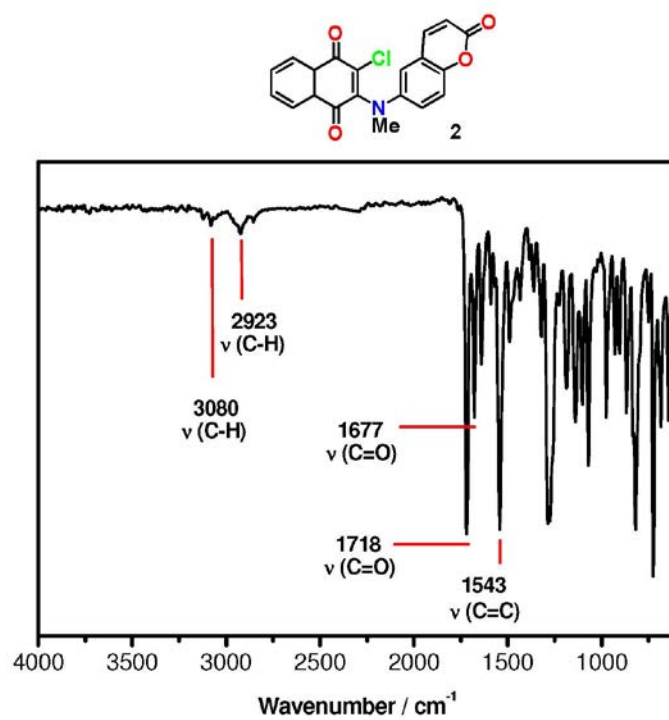
Figure S5. FTIR spectrum of compound **2** (KBr).
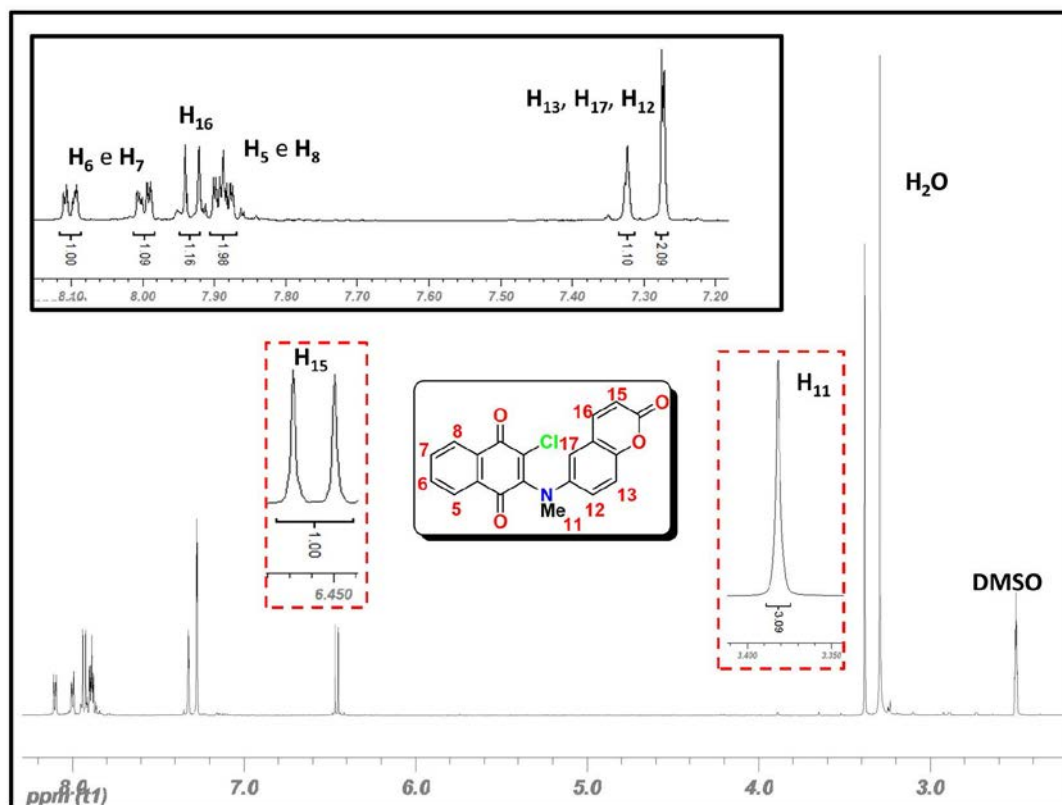
Figure S6. ^{1}H NMR spectrum of **2** in DMSO-d$_6$ (500 MHz).
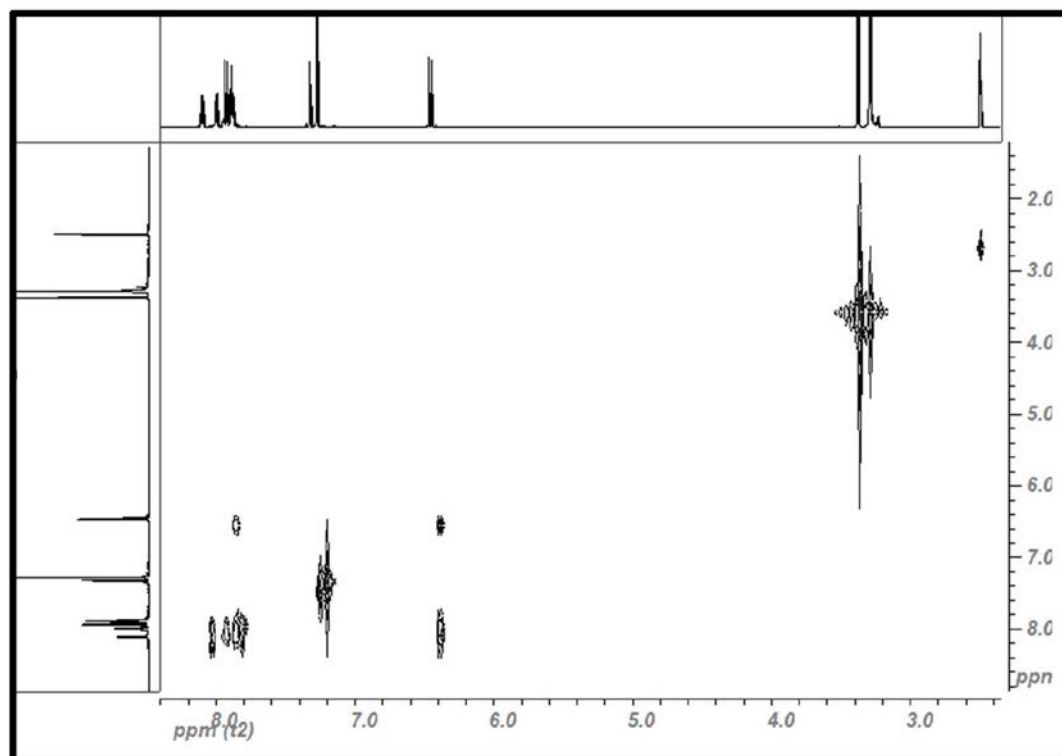
Figure S7. ^{1}H × ^{1}H – COSY of **2** in DMSO-d$_6$ (500MHz).
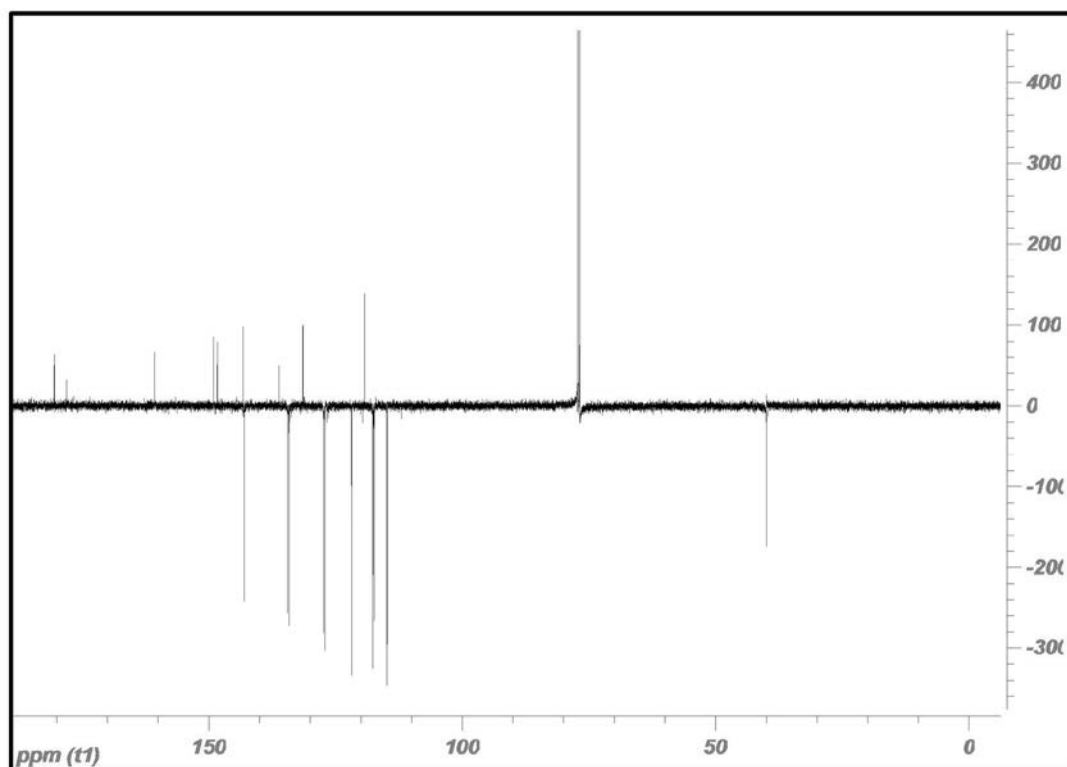
Figure S8. ¹³C NMR-APT spectrum of **2** in CDCl₃ (75 MHz).

1.3. 2-(2-oxo-2H-chromen-6-ylamino)-3-(propylthio)naphthalene-1,4-dione **3**
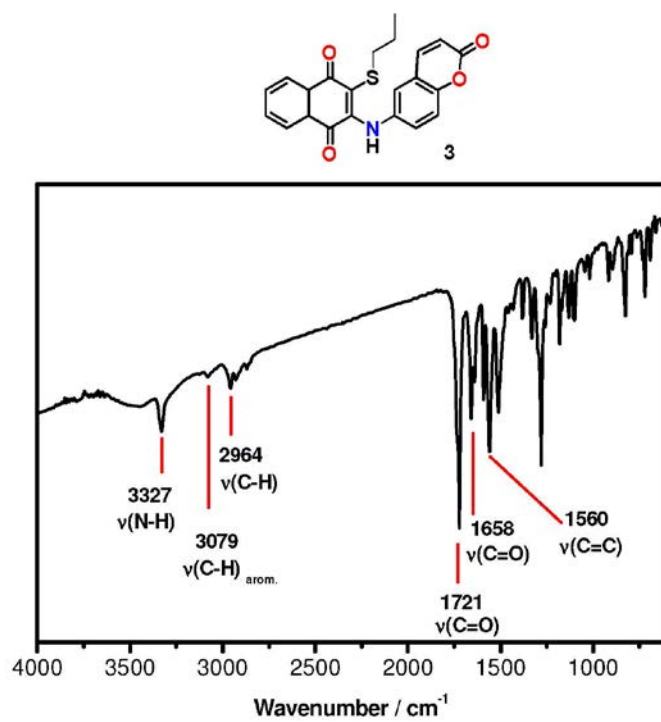
Figure S9. FTIR spectrum of compound **3** (KBr).
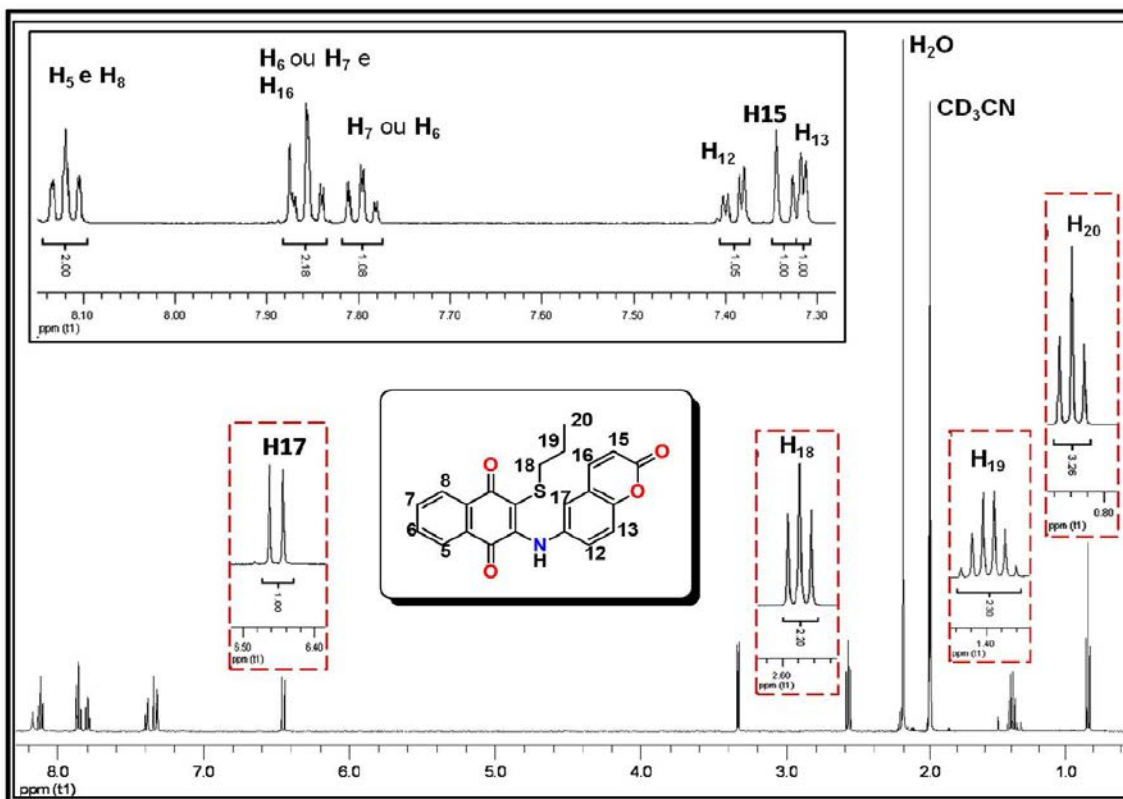
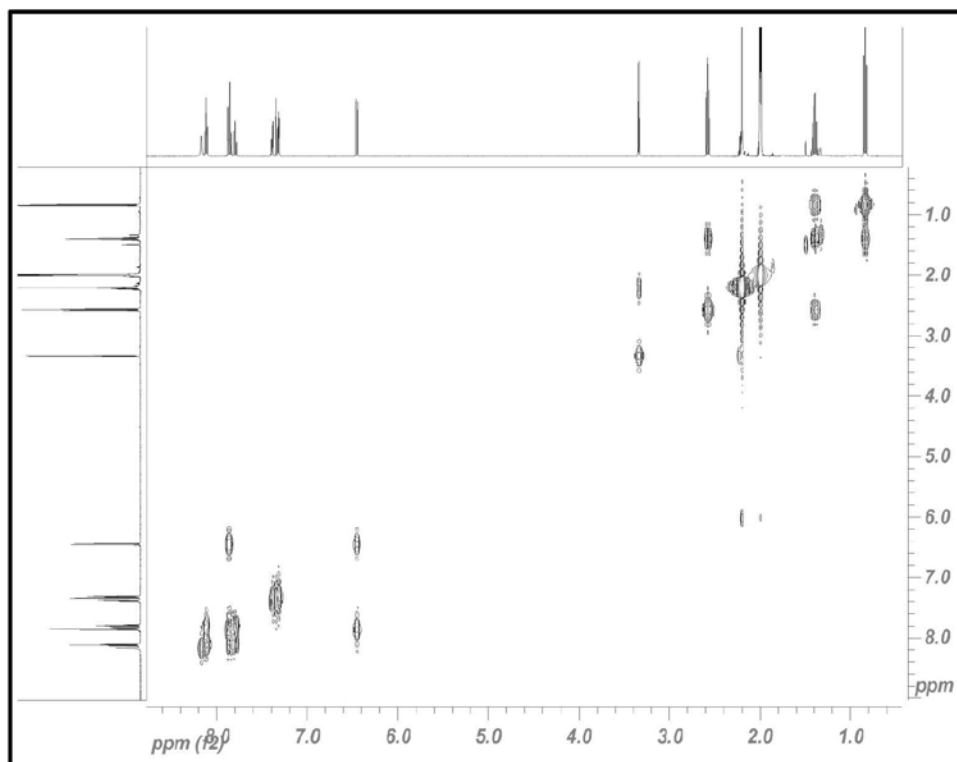**Figure S10.** ^{1}H NMR spectrum of **3** in CD_3CN (500 MHz).
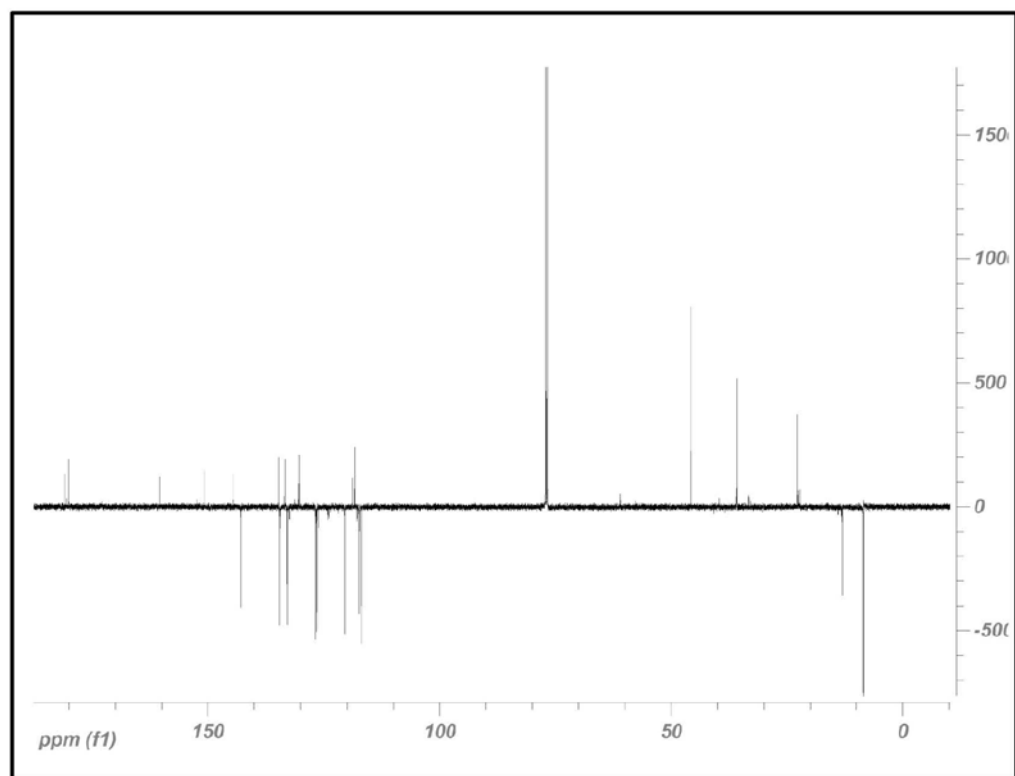

Figure S11. ^{1}H × ^{1}H – COSY of **3** in CD_3CN (500 MHz).

Figure S12. ¹³C NMR-APT spectrum of **3** in CDCl₃ (75 MHz).

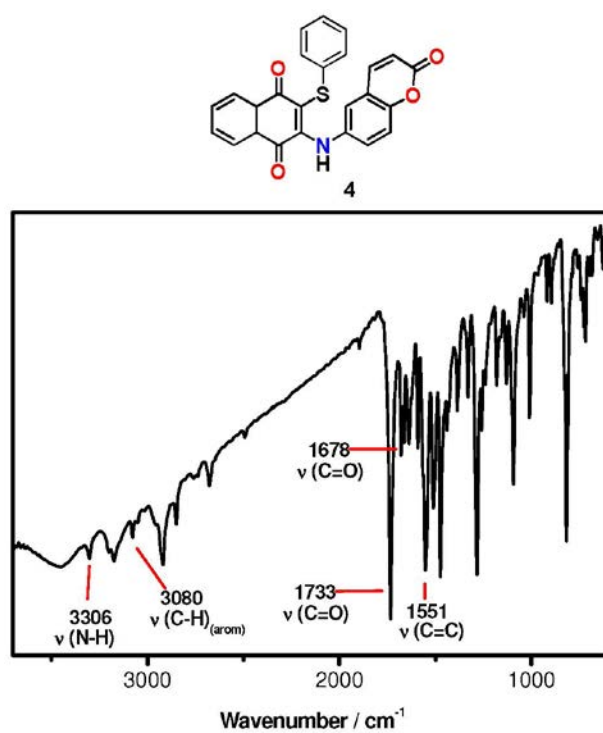1.4. 2-(2-oxo-2H-chromen-6-ylamino)-3-(phenylthiol)naphthalene-1,4(4aH,8aH)-dione **4**

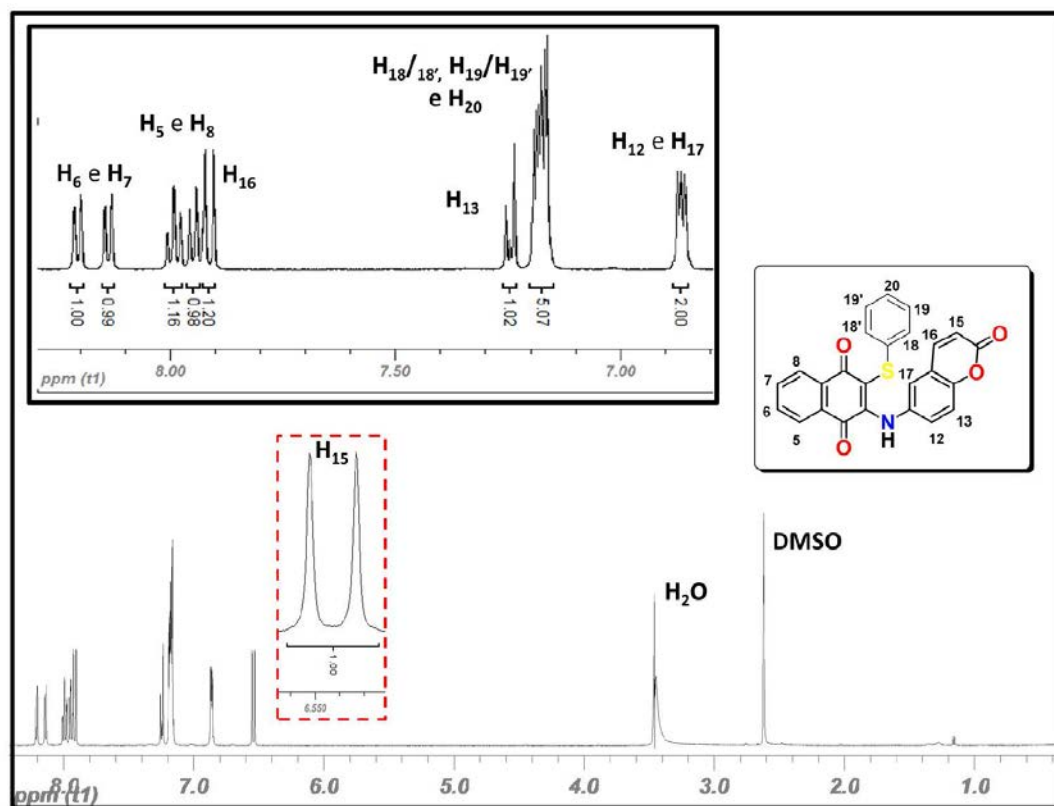**Figure S13.** FTIR spectrum of compound **4** (KBr).

Figure S14 ¹H NMR spectrum of **4** in DMSO-d₆. (500 MHz).

Figure S15. ¹H × ¹H – COSY of **4** in DMSO-d₆ (500 MHz).

1.5. 2-(4-chlorophenylthiol)-3-(2-oxo-2H-chromen-6-ylamino)naphthalene-1,4(4aH, 8aH)-dione **5**
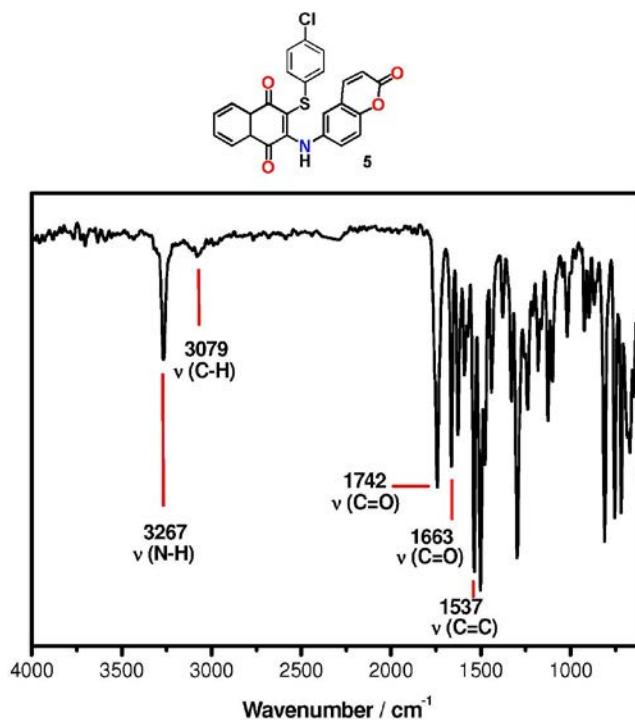
Figure S16. FTIR spectrum of compound **5** (KBr).

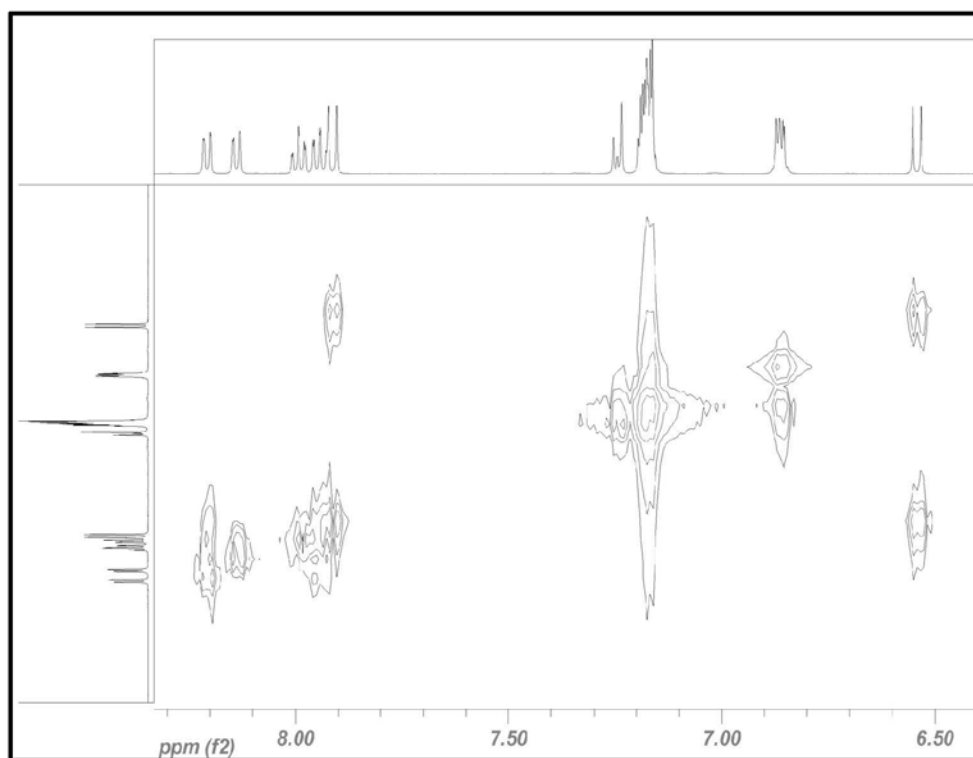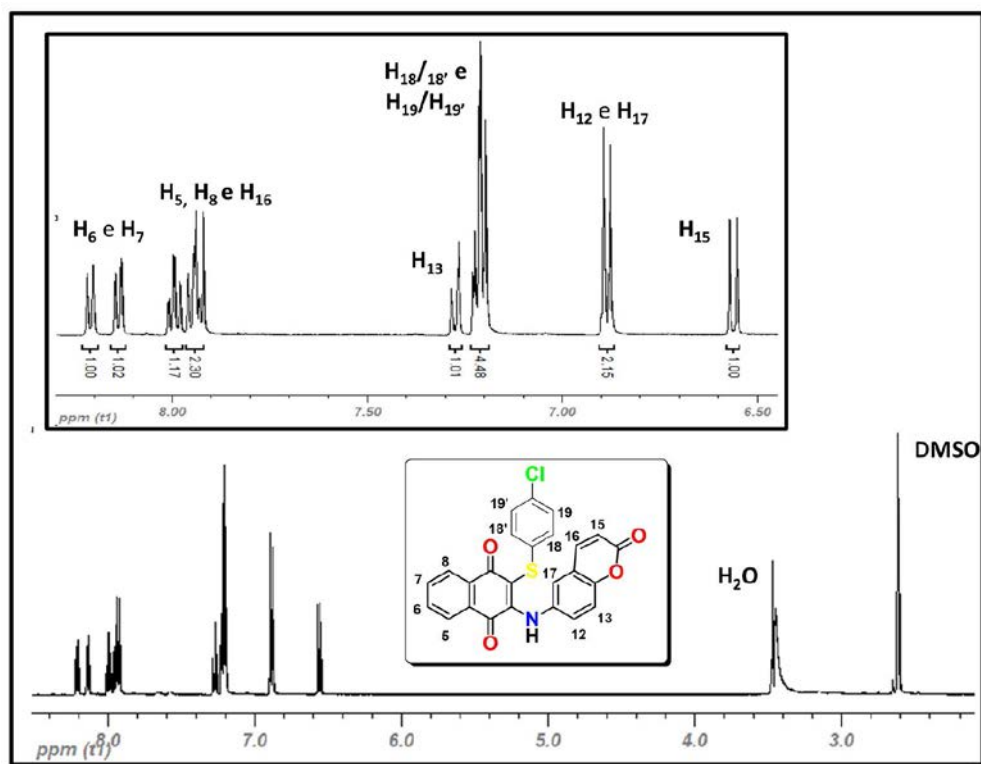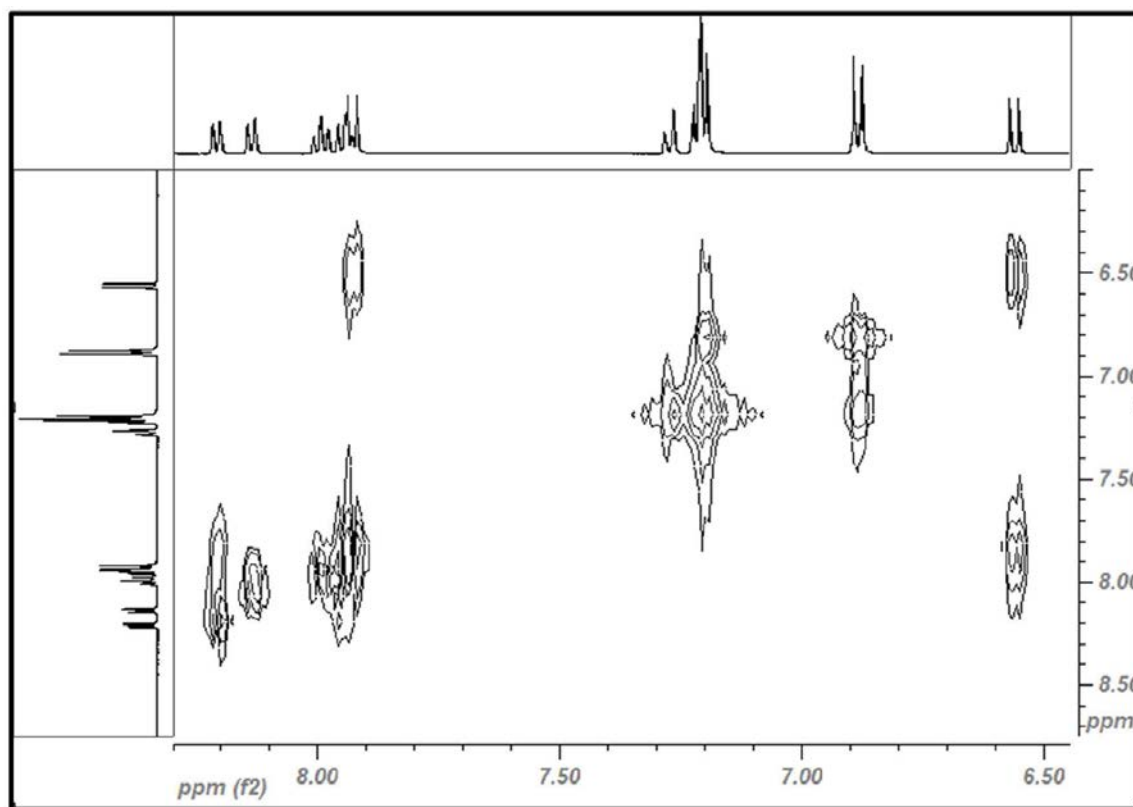**Figure S17.** ^{1}H NMR spectrum of **5** in DMSO-d$_6$ (500 MHz).

Figure S18. $^1H \times {}^1H$ – COSY of **5** in DMSO-d$_6$ (500 MHz).

2. Cyclic voltammograms

Obtained with a BAS Epsilon potentiostat–galvanostat system at room temperature, using *n*-Bu$_4$NClO$_4$ (0.1 mol L^{-1}) as the supporting electrolyte in CH$_3$CN (spectroscopic grade) solutions of the compounds (at 1.0×10^{-3} mol L^{-1}). The electrochemical cell was a conventional one with three electrodes: Ag/Ag$^+$ was used as the reference electrode, a platinum wire as the auxiliary electrode and glassy carbon as the working electrode. The ferrocene/ferrocenium (FcH/FcH$^+$) couple was used as the internal standard. Pure argon was bubbled through the electrolytic solution to remove oxygen in all experiments. The potential scan was initiated in the anodic direction. Both anodic and cathodic peaks are indicated in the voltammograms.
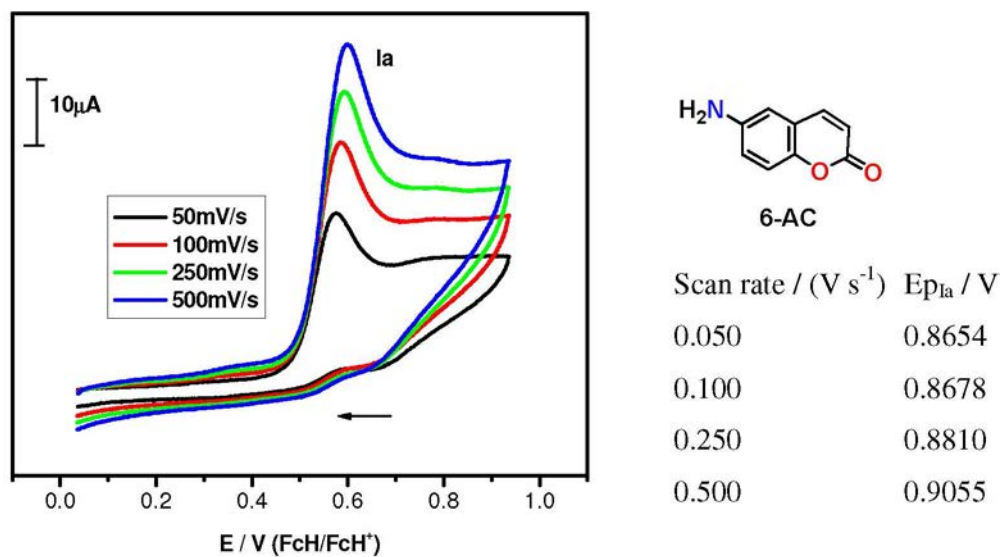
Figure S19. Cyclic voltammograms of 6-aminocoumarin 6-AC; values *vs.* FcH/FcH⁺.

Scan rate / (V s⁻¹)	Ep_Ia / V
0.050	0.8654
0.100	0.8678
0.250	0.8810
0.500	0.9055
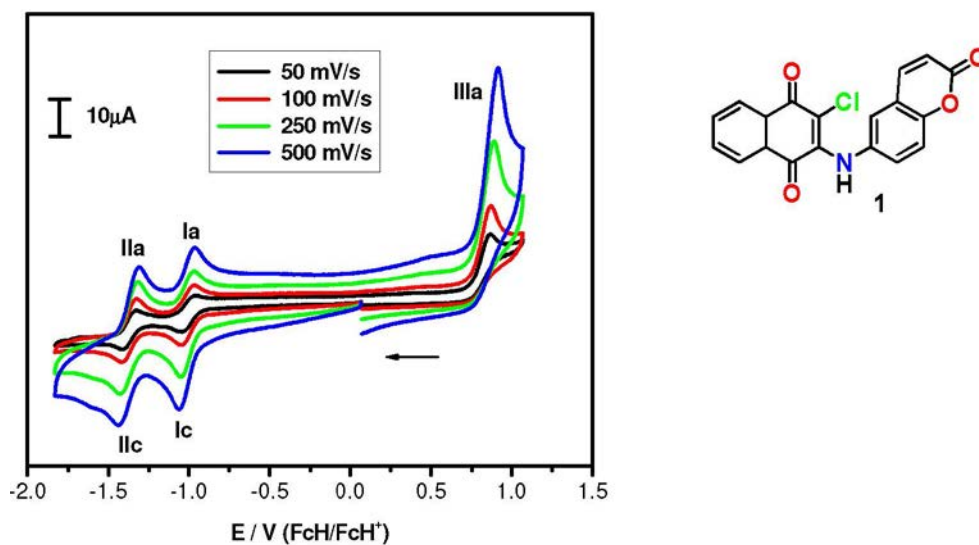
Scan rate / (V s⁻¹)	EpIc / V	EpIa / V	EpIIc / V	EpIIa / V	EpIIIa / V	EpI / V	EpII / V	E½pI / V	E½pII / V
0.050	−1.038	−0.961	−1.420	−1.328	0.865	0.077	0.093	0.999	1.374
0.100	−1.038	−0.961	−1.420	−1.328	0.868	0.077	0.093	0.999	1.374
0.250	−1.049	−0.972	−1.431	−1.328	0.881	0.077	0.103	1.010	1.379
0.500	−1.059	−0.961	−1.447	−1.317	0.906	0.097	0.125	1.001	1.379

Figure S20. Cyclic voltammograms of 2-chloro-3-(2-oxo-2H-chromen-6-ylamino)naphthalene-1,4-dione **1**; values *vs.* FcH/FcH⁺.
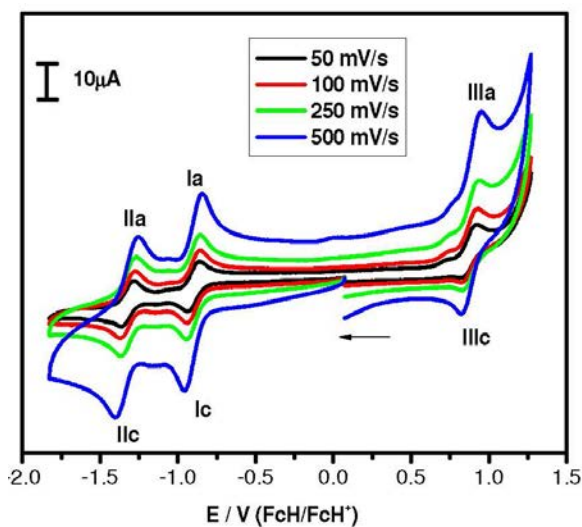
Scan rate / (V s⁻¹)	EpIc / V	EpIa / V	EpIIc / V	EpIIa / V	EpIIIc / V	EpIIIa / V	ΔEpI / V	ΔEpII / V	ΔEpIII / V	E½pI / V	E½pII / V	E½pIII / V
0.050	−0.943	−0.868	−1.409	−1.276	0.835	0.920	0.075	0.133	0.085	−0.905	−1.342	0.877
0.100	−0.953	−0.857	−1.367	−1.273	0.835	0.921	0.096	0.094	0.086	−0.905	−1.320	0.878
0.250	−0.952	−0.857	−1.372	−1.274	0.825	0.931	0.095	0.098	0.106	−0.904	−1.323	0.878
0.500	−0.964	−0.855	−1.374	−1.268	0.814	0.947	0.109	0.106	0.133	−0.909	−1.321	0.880

**Figure S21.** Cyclic voltammogram of 2-chloro-3-(methyl(2-oxo-2H-chromen-6-yl)amino)-naphthalene-1,4-dione **2**; values *vs.* FcH/FcH⁺.
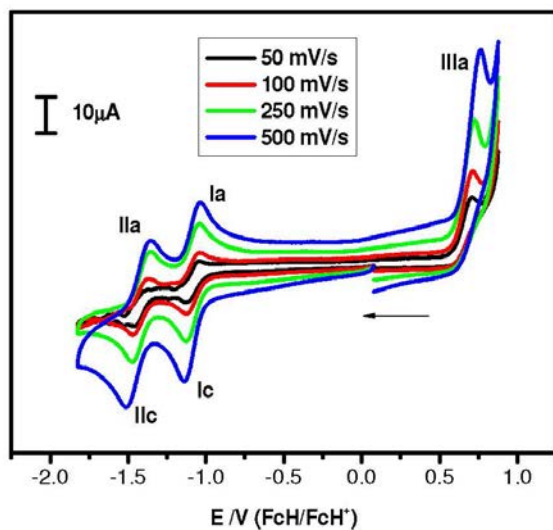
Scan rate / (V s⁻¹)	EpIc / V	EpIa / V	EpIIc / V	EpIIa / V	EpIIIa / V	ΔEpI / V	ΔEpII / V	E½pI / V	E½pII / V
0.050	−1.121	−1.046	−1.462	−1.374	0.705	0.075	0.088	1.083	1.418
0.100	−1.121	−1.047	−1.472	−1.372	0.710	0.074	0.100	1.084	1422
0.250	−1.121	−1.046	−1.479	−1.362	0.721	0.075	0.117	1.083	1.420
0.500	−1.142	−1.035	−1.521	−1.359	0.763	0.107	0.162	1.088	1.440

Figure S22. Cyclic voltammogram of 2-(2-oxo-2H-chromen-6-ylamino)-3-(propylthio)-naphthalene-1,4-dione **3**; values *vs.* FcH/FcH⁺.
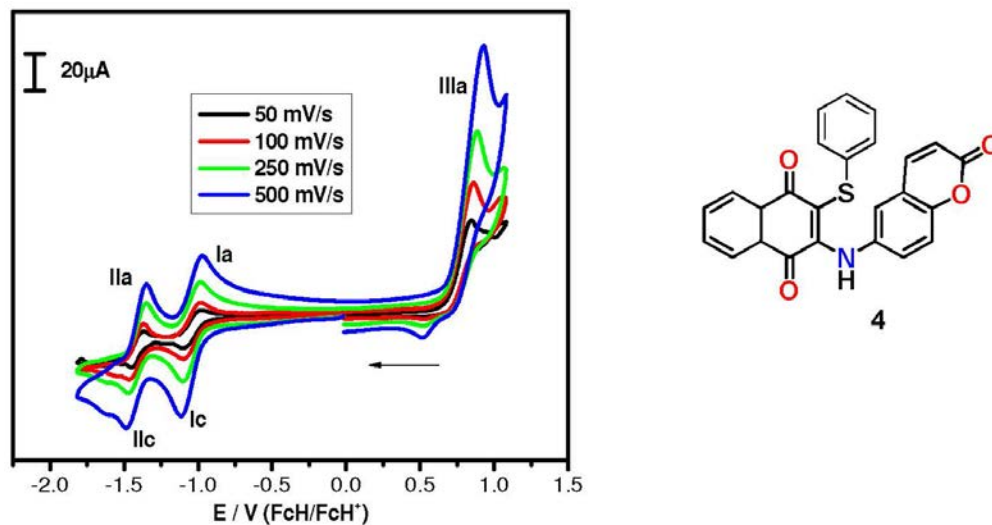
Scan rate / (V s⁻¹)	EpIc / V	EpIa / V	EpIIc / V	EpIIa / V	EpIIIa / V	ΔEpI / V	ΔEpII / V	E½pI / V	E½pII / V
0.050	−1.106	−0.984	−1.449	−1.369	0.840	0.122	0.080	−1.045	−1.409
0.100	−1.107	−0.984	−1.472	−1.368	0.863	0.123	0.104	−1.045	−1.420
0.250	−1.106	−0.984	−1.472	−1.358	0.885	0.122	0.114	−1.045	−1.415
0.500	−1.117	−0.972	−1.495	−1.346	0.920	0.145	0.149	−1.044	−1.420

Figure S23. Cyclic voltammogram of 2-(2-oxo-2H-chromen-6-ylamino)-3-(phenylthiol)-naphthalene-1,4(4aH,8aH)-dione **4**; values *vs.* FcH/FcH⁺.
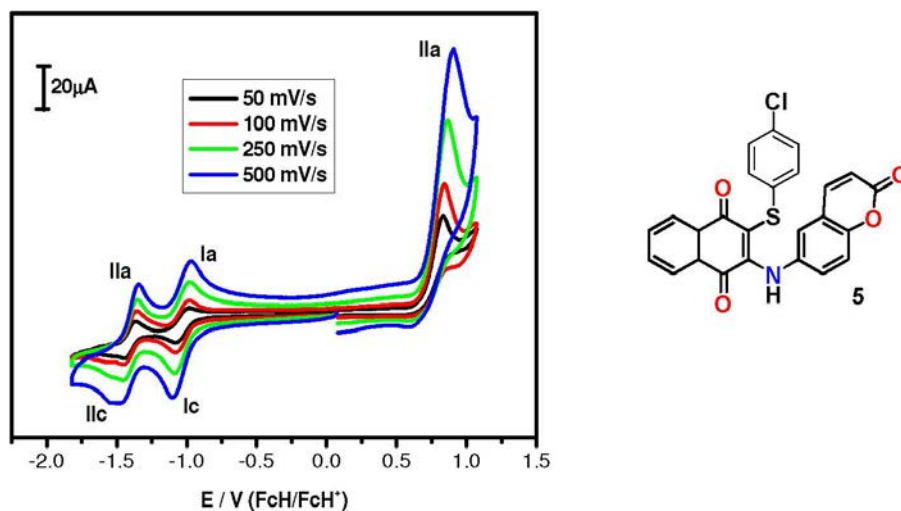
Scan rate / (V s⁻¹)	EpIc / V	EpIa / V	EpIIc / V	EpIIa / V	EpIIIa / V	EpI / V	EpII / V	E½pI / V	E½pII / V
0.050	−1.079	−0.988	−1.443	−1.363	0.831	0.091	0.080	−1.033	−1.403
0.100	−1.087	−0.985	−1.455	−1.360	0.842	0.102	0.095	−1.036	−1.407
0.250	−1.091	−0.977	−1.455	−1.360	0.854	0.114	0.095	−1.034	−1.407
0.500	−1.102	−0.977	−1.458	−1.352	0.900	0.125	0.106	−1.039	−1.405

Figure S24. Cyclic voltammogram of 2-(4-chlorophenylthiol)-3-(2-oxo-2H-chromen-6-ylamino)-naphthalene-1,4(4aH, 8aH)-dione **5**; values *vs.* FcH/FcH⁺.

3. Computational details

**Table S1.** Selected bond lengths (Å) for the ground (S_0) and excited (S_1) states of compounds **1-4**

1 - R^1 = Cl, R^2 = H
2 - R^1 = Cl, R^2 = CH₃
3 - R^1 = S^{i}Pr, R^2 = H
4 - R^1 = SPh, R^2 = H
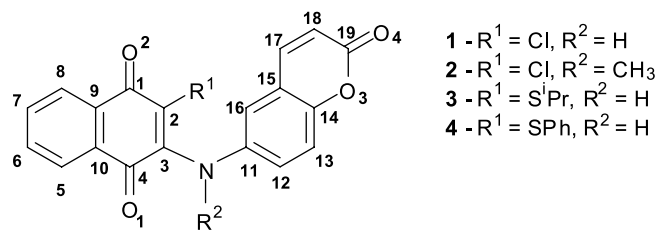
Bond	X-ray	1		2		3		4	
		S_0	S_1	S_0	S_1	S_0	S_1	S_0	S_1
C1–C2	1.461	1.466	1.445	1.484	1.445	1.475	1.453	1.474	1.453
C2–C3	1.356	1.375	1.390	1.369	1.389	1.381	1.392	1.381	1.392
C2–R^1	1.727	1.747	1.751	1.739	1.751	1.782	1.783	1.786	1.783
C3–N1	1.361	1.359	1.432	1.391	1.441	1.365	1.438	1.360	1.438
N1–R^2	0.880	1.019	1.017	1.471	1.472	1.018	1.017	1.018	1.017
C3–C4	1.511	1.518	1.441	1.514	1.440	1.511	1.439	1.516	1.441
C4–O1	1.214	1.229	1.262	1.227	1.262	1.232	1.264	1.231	1.263
C4–C10	1.474	1.474	1.474	1.483	1.474	1.475	1.473	1.473	1.474
C10–C5	1.389	1.401	1.409	1.400	1.409	1.400	1.410	1.401	1.409
C5–C6	1.383	1.395	1.388	1.396	1.388	1.395	1.388	1.395	1.388
C6–C7	1.379	1.399	1.408	1.400	1.408	1.399	1.408	1.399	1.408
C7–C8	1.392	1.398	1.388	1.396	1.388	1.398	1.388	1.398	1.388
C8–C9	1.384	1.397	1.410	1.399	1.410	1.397	1.410	1.397	1.410
C9–C10	1.406	1.407	1.418	1.407	1.418	1.406	1.418	1.407	1.418
C9–C1	1.492	1.496	1.479	1.488	1.479	1.499	1.479	1.499	1.481
C1–O2	1.220	1.234	1.258	1.230	1.258	1.236	1.260	1.234	1.256
C11–N1	1.411	1.416	1.343	1.410	1.355	1.417	1.346	1.420	1.348
C11–C12	1.398	1.410	1.437	1.414	1.436	1.410	1.435	1.408	1.435
C12–C13	1.370	1.389	1.368	1.391	1.372	1.389	1.370	1.390	1.371
C13–C14	1.376	1.396	1.414	1.393	1.411	1.395	1.412	1.395	1.412
C14–O3	1.387	1.372	1.343	1.374	1.346	1.373	1.346	1.372	1.346
O3–C19	1.386	1.384	1.410	1.381	1.408	1.383	1.407	1.384	1.407
C19–O4	1.198	1.221	1.210	1.223	1.211	1.222	1.211	1.221	1.211
C19–C18	1.447	1.453	1.454	1.453	1.454	1.453	1.454	1.453	1.454
C18–C17	1.332	1.356	1.351	1.356	1.352	1.356	1.352	1.356	1.352
C17–C15	1.447	1.441	1.446	1.442	1.446	1.441	1.445	1.441	1.445
C15–C14	1.385	1.406	1.420	1.406	1.416	1.406	1.418	1.407	1.418
C15–C16	1.396	1.407	1.387	1.404	1.388	1.407	1.389	1.407	1.389
C16–C11	1.380	1.393	1.423	1.400	1.425	1.394	1.421	1.393	1.420
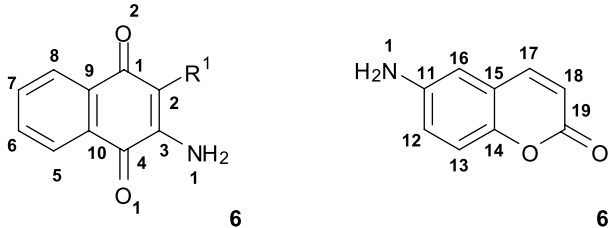
Table S2. Selected bond lengths (Å) for the ground state (S_0) of compounds **3-5**

3 - R^1 = S^iPr, R^2 = H
4 - R^1 = SPh, R^2 = H
5 - R^1 = $S(C_6H_4Cl)$, R^2 = H
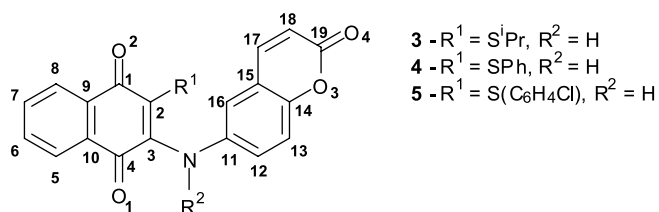
Bond	3	4	5
C1–C2	1.475	1.474	1.474
C2–C3	1.381	1.381	1.381
C2–R^1	1.782	1.786	1.786
C3–N1	1.365	1.360	1.359
N1–R^2	1.018	1.018	1.019
C3–C4	1.511	1.516	1.517
C4–O1	1.232	1.231	1.230
C4–C10	1.475	1.473	1.473
C10–C5	1.400	1.401	1.401
C5–C6	1.395	1.395	1.395
C6–C7	1.399	1.399	1.399
C7–C8	1.398	1.398	1.398
C8–C9	1.397	1.397	1.397
C9–C10	1.406	1.407	1.407
C9–C1	1.499	1.499	1.499
C1–O2	1.236	1.234	1.234
C11–N1	1.417	1.420	1.421
C11–C12	1.410	1.408	1.408
C12–C13	1.389	1.390	1.390
C13–C14	1.395	1.395	1.395
C14–O3	1.373	1.372	1.372
O3–C19	1.383	1.384	1.384
C19–O4	1.222	1.221	1.221
C19–C18	1.453	1.453	1.453
C18–C17	1.356	1.356	1.356
C17–C15	1.441	1.441	1.441
C15–C14	1.406	1.407	1.407
C15–C16	1.407	1.407	1.406
C16–C11	1.394	1.393	1.393

Table S3. Mulliken charges for the ground (S_0) and excited (S_1) states of compounds 1-4
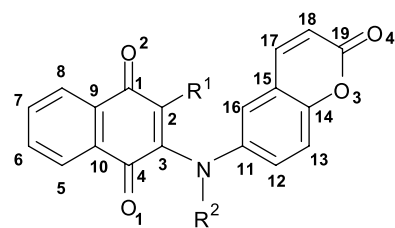

1 - R^1 = Cl, R^2 = H
2 - R^1 = Cl, R^2 = CH_3
3 - R^1 = S^iPr, R^2 = H
4 - R^1 = SPh, R^2 = H
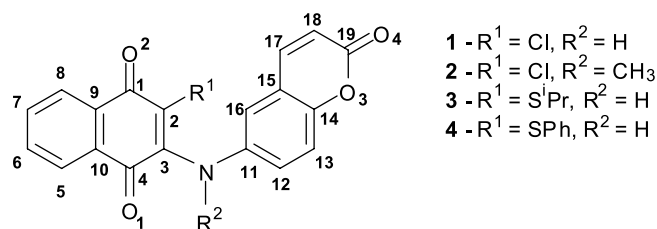
Atom	1		2		3		4	
	S_0	S_1	S_0	S_1	S_0	S_1	S_0	S_1
C1	−0.457	0.110	0.133	0.157	0.228	0.001	0.224	−0.012
O2	−0.504	−0.655	−0.516	−0.656	−0.516	−0.613	−0.437	−0.574
C2	0.741	−0.006	−0.049	−0.246	−0.020	0.127	−0.299	0.297
R^1	0.214	0.191	0.247	0.221	0.159	0.342	−0.138	0.256
C3	0.196	−0.120	−0.925	−0.737	−0.152	0.072	−0.334	−0.508
N1	−0.258	−0.181	0.224	0.442	−0.181	−0.196	−0.223	−0.219
R^2	0.357	0.375	−0.101	−0.035	0.357	0.368	0.361	0.363
C4	−0.556	0.005	0.020	0.278	0.199	0.066	0.293	0.331
O1	−0.540	−0.637	−0.458	−0.590	−0.524	−0.667	−0.515	−0.679
C5	−0.045	0.099	0.017	−0.201	0.135	0.011	−0.010	−0.222
C6	−0.200	−0.145	−0.095	−0.146	−0.191	−0.189	−0.195	−0.169
C7	−0.173	−0.197	−0.168	−0.193	−0.165	−0.117	−0.140	−0.163
C8	−0.058	−0.089	−0.037	−0.152	0.167	0.074	0.257	−0.026
C9	0.296	0.062	0.305	0.161	−0.168	−0.014	0.015	−0.165
C10	0.326	0.450	0.292	0.188	−0.107	−0.197	−0.067	0.091
C11	−0.189	−0.377	0.217	0.194	−0.214	−0.042	−0.115	−0.248
C12	0.297	−0.239	−0.287	−0.198	0.156	0.172	0.236	0.168
C13	−0.351	0.113	−0.205	−0.355	−0.265	−0.324	−0.495	−0.335
C14	−1.395	−1.705	−1.551	−1.755	−1.224	−1.208	−1.070	−1.213
C15	1.744	1.889	1.688	1.726	1.690	1.769	1.834	1.866
C16	−0.224	0.010	0.068	0.166	−0.202	−0.248	−0.298	−0.179
O3	−0.423	−0.368	−0.428	−0.375	−0.431	−0.415	−0.431	−0.422
C17	−0.399	−0.249	−0.419	−0.048	−0.431	−0.534	−0.510	−0.451
C18	0.065	0.010	0.017	−0.095	0.136	0.178	0.145	0.160
C19	0.588	0.594	0.594	0.607	0.577	0.564	0.588	0.581
O4	−0.555	−0.489	−0.560	−0.498	−0557	−0.533	−0.554	−0.548

Table S4. Selected bond lengths (Å) for the ground (S$_0$) and excited (S$_1$) states of the individual molecules


Bond	6-AC		6	
	S$_0$	S$_1$	S$_0$	S$_1$
C1–C2	–	–	1.453	1.481
C2–C3	–	–	1.374	1.422
C2–R^1	–	–	1.753	1.708
C3–N1	–	–	1.339	1.321
N1–R^2	1.012	1.011	1.011	1.018
C3–C4	–	–	1.513	1.488
C4–O1	–	–	1.228	1.267
C4–C10	–	–	1.476	1.432
C10–C5	–	–	1.400	1.421
C5–C6	–	–	1.396	1.378
C6–C7	–	–	1.398	1.423
C7–C8	–	–	1.398	1.378
C8–C9	–	–	1.396	1.419
C9–C10	–	–	1.409	1.446
C9–C1	–	–	1.501	1.449
C1–O2	–	–	1.237	1.249
C11–N	1.396	1.351	–	–
C11–C12	1.416	1.422	–	–
C12–C13	1.390	1.385	–	–
C13–C14	1.394	1.411	–	–
C14–O3	1.378	1.359	–	–
O3–C19	1.377	1.459	–	–
C19–O4	1.225	1.235	–	–
C19–C18	1.453	1.406	–	–
C18–C17	1.357	1.406	–	–
C17–C15	1.441	1.432	–	–
C15–C14	1.406	1.426	–	–
C15–C16	1.408	1.399	–	–
C16–C11	1.398	1.428	–	–

**Table S5.** Mulliken charges for the ground (S_0) and excited (S_1) states of individual molecules
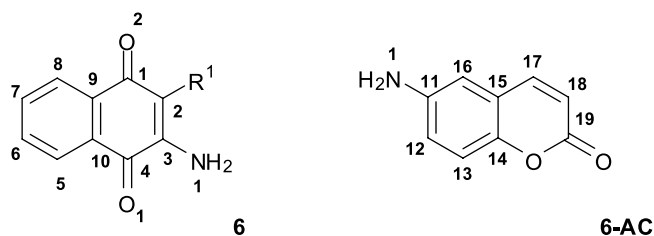
Atom	6-AC		6	
	S_0	S_1	S_0	S_1
C1	–	–	−0.244	−0.362
O2	–	–	−0.568	−0.619
C2	–	–	0.145	0.360
R¹	–	–	0.178	0.332
C3	–	–	0.884	0.786
N1	−0.617	−0.493	−0.633	−0.519
R²	0.317	0.363	0.350	0.368
C4	–	–	−0.830	−0.923
O1	–	–	−0.505	−0.663
C5	–	–	0.197	0.100
C6	–	–	−0.201	−0.164
C7	–	–	−0.216	−0.214
C8	–	–	0.105	0.032
C9	–	–	0.044	0.106
C10	–	–	0.281	0.374
C11	−0.101	0.002	–	–
C12	0.275	0.227	–	–
C13	−0.246	−0.238	–	–
C14	−1.686	−1.634	–	–
C15	1.218	1.150	–	–
C16	−0.030	−0.007	–	–
O3	−0.426	−0.451	–	–
C17	0.197	0.143	–	–
C18	−0.024	−0.113	–	–
C19	0.592	0.551	–	–
O4	−0.580	−0.631	–	–

Table S6. Percent S_0–S_1 bond distance differences
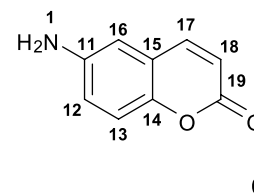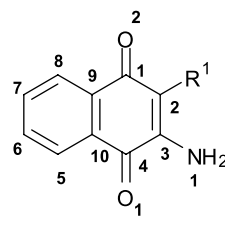
| Bond	1	2	3	4	6-AC	6
C1–C2	−1.4	−2.6	−1.5	−1.4		1.9
C2–C3	1.1	1.5	0.8	0.8		3.5
C2–R1	0.2	0.7	0.1	−0.2		−2.6
C3–N1	5.4	3.6	5.3	5.7		−1.3
N1–R2	−0.2	0.1	−0.1	−0.1	−0.1	0.7
C3–C4	−5.1	−4.9	−4.8	−4.9		−1.7
C4–O1	2.7	2.9	2.6	2.6		3.2
C4–C10	0.0	−0.6	−0.1	0.1		−3.0
C10–C5	0.6	0.6	0.7	0.6		1.5
C5–C6	−0.5	−0.6	−0.5	−0.5		−1.3
C6–C7	0.6	0.6	0.6	0.6		1.8
C7–C8	−0.7	−0.6	−0.7	−0.7		−1.4
C8–C9	0.9	0.8	0.9	0.9		1.6
C9–C10	0.8	0.8	0.9	0.8		2.6
C9–C1	−1.1	−0.6	−1.3	−1.2		−3.5
C1–O2	1.9	2.3	1.9	1.8		1.0
C11–N1	−5.2	−3.9	−5.0	−5.1	−3.2	
C11–C12	1.9	1.6	1.8	1.9	0.4	
C12–C13	−1.5	−1.4	−1.4	−1.4	−0.4	
C13–C14	1.3	1.3	1.2	1.2	1.2	
C14–O3	−2.1	−2.0	−2.0	−1.9	−1.4	
O3–C19	1.9	2.0	1.7	1.7	6.0	
C19–O4	−0.9	−1.0	−0.9	−0.8	0.8	
C19–C18	0.1	0.1	0.1	0.1	−3.2	
C18–C17	−0.4	−0.3	−0.3	−0.3	3.6	
C17–C15	0.3	0.3	0.3	0.3	−0.6	
C15–C14	1.0	0.7	0.9	0.8	1.4	
C15–C16	−1.4	−1.1	−1.3	−1.3	−0.6	
C16–C11	2.2	1.8	1.9	1.9	2.1	
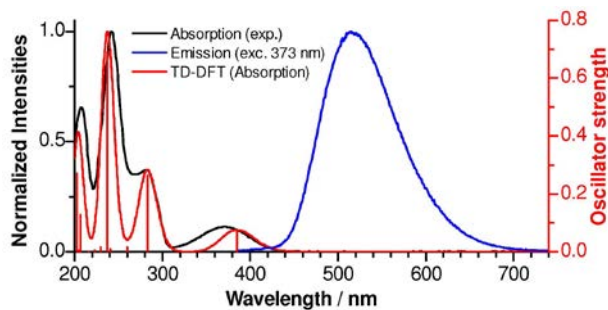
Figure S25. Simulated electronic spectrum (TD-DFT – B3LYP/6-31+G(d,p)/PCM(CH$_3$CN)) of compound 6-AC (red) and experimental absorption (black) and emission (blue) spectra.
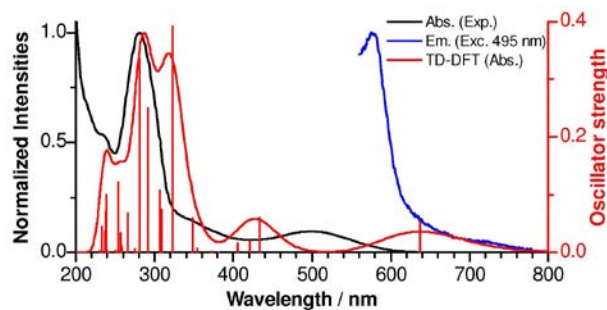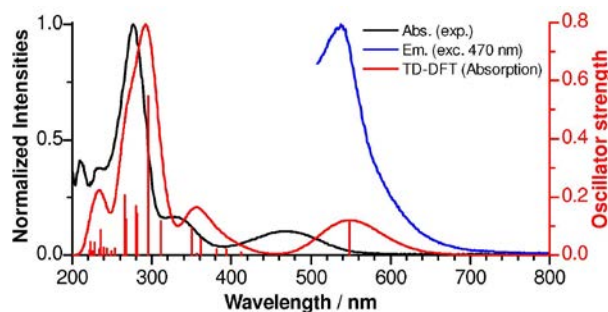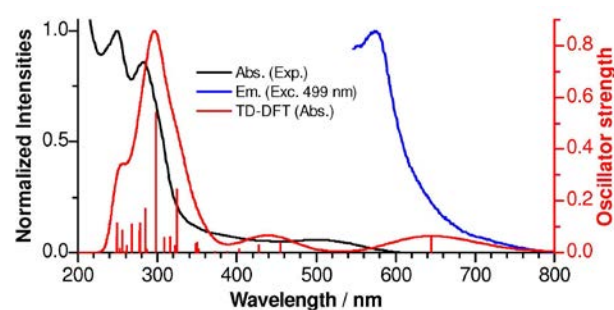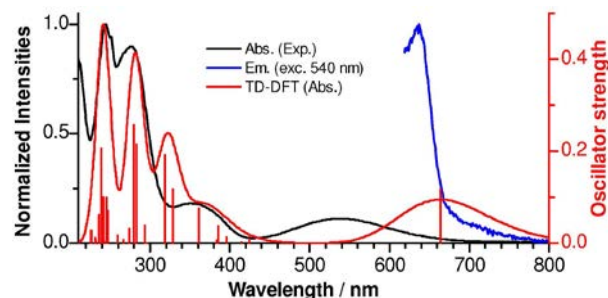

Figure S29. Simulated electronic spectrum (TD-DFT – B3LYP/6-31+G(d,p)/PCM(CH$_3$CN)) of compound **3** (red) and experimental absorption (black) and emission (blue) spectra.
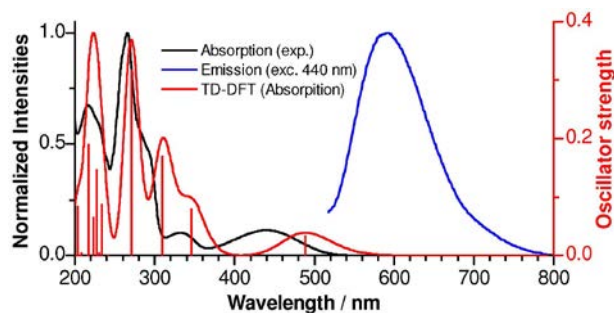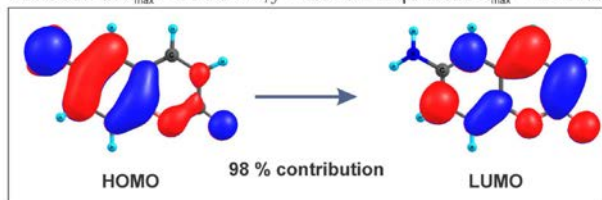

Figure S26. Simulated electronic spectrum (TD-DFT – B3LYP/6-31+G(d,p)/PCM(CH$_3$CN)) of compound **6** (red) and experimental absorption (black) and emission (blue) spectra.
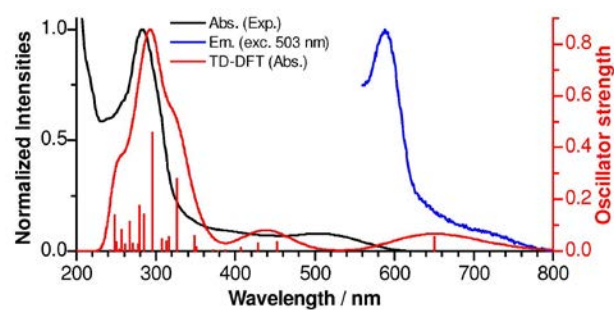
Figure S30. Simulated electronic spectrum (TD-DFT – B3LYP/6-31+G(d,p)/PCM(CH$_3$CN)) of compound **4** (red) and experimental absorption (black) and emission (blue) spectra.

Figure S27. Simulated electronic spectrum (TD-DFT – B3LYP/6-31+G(d,p)/PCM(CH$_3$CN)) of compound **1** (red) and experimental absorption (black) and emission (blue) spectra.

Figure S31. Simulated electronic spectrum (TD-DFT – B3LYP/6-31+G(d,p)/PCM(CH$_3$CN)) of compound **5** (red) and experimental absorption (black) and emission (blue) spectra.

Figure S28. Simulated electronic spectrum (TD-DFT – B3LYP/6-31+G(d,p)/PCM(CH$_3$CN)) of compound **2** (red) and experimental absorption (black) and emission (blue) spectra.
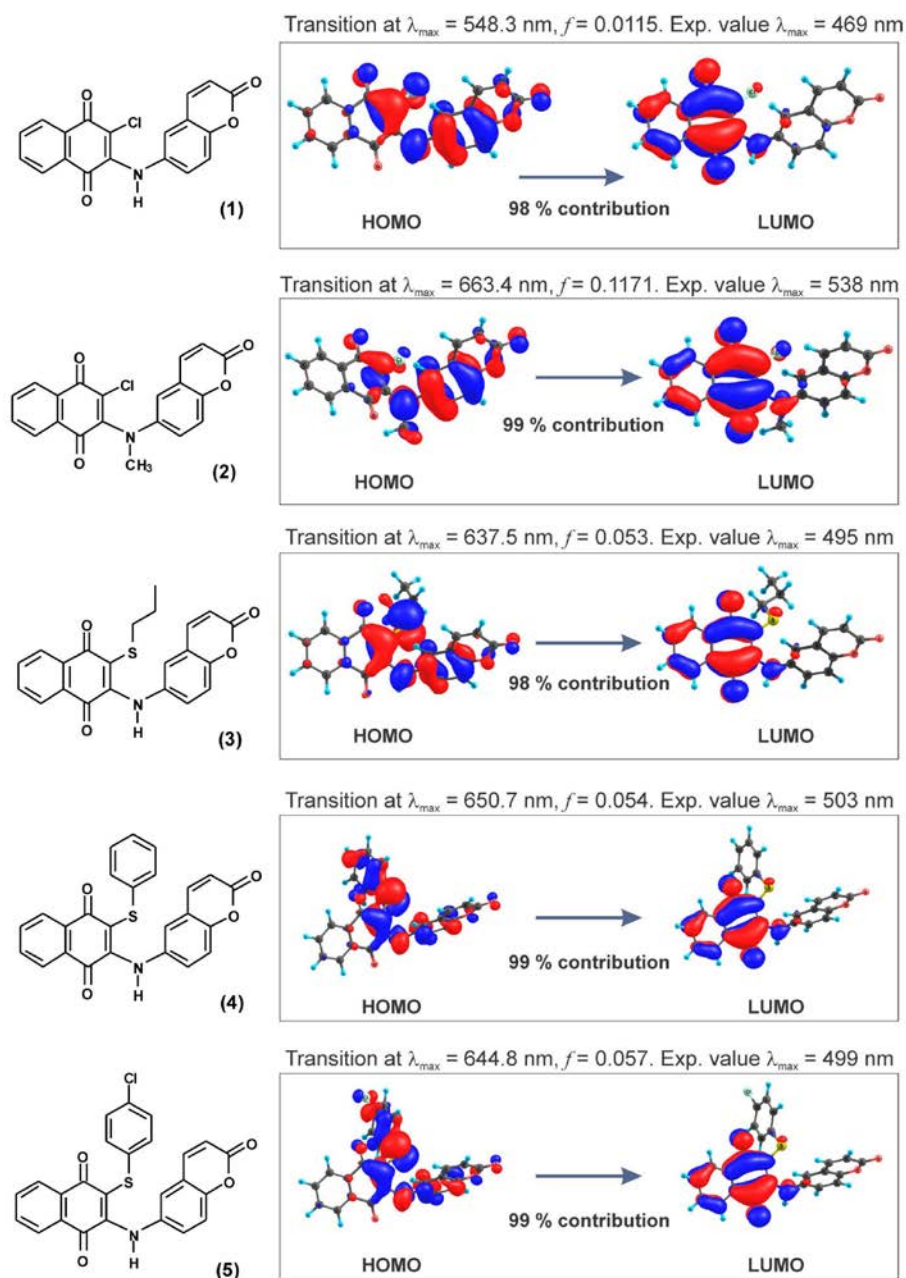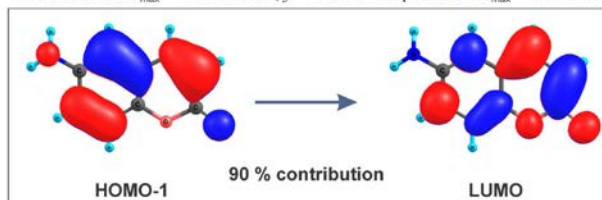
Figure S32. Molecular orbitals of **1-5** involved in the lowest energy transition (contour values plotted at 0.03 (e/Bohr^3)$^{1/2}$).
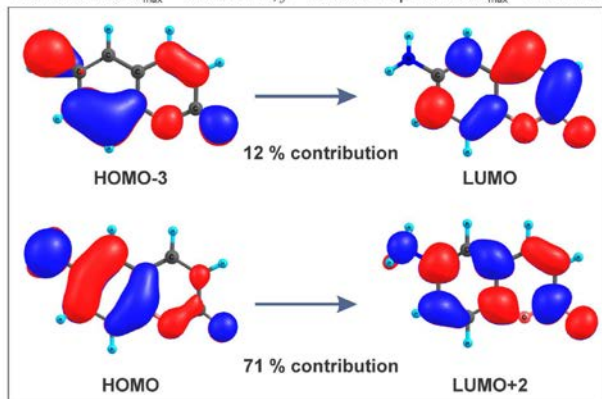
Transition at λ_{max} = 384.6 nm, f = 0.0707. Exp. value λ_{max} = 373 nm

HOMO   98 % contribution   LUMO

Transition at λ_{max} = 283.0 nm, f = 0.263. Exp. value λ_{max} = 282 nm

HOMO-1   90 % contribution   LUMO

Transition at λ_{max} = 237.2 nm, f = 0.691. Exp. value λ_{max} = 272 nm

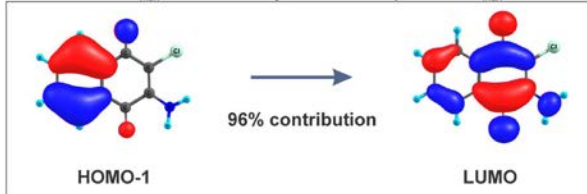HOMO-3   12 % contribution   LUMO

HOMO   71 % contribution   LUMO+2

Figure S33. Molecular orbitals of 6-AC involved in the three lowest energy electronic transitions (contour values plotted at 0.03 (e/Bohr^3)$^{1/2}$).

Transition at λ_{max} = 488.7 nm, f = 0.033. Exp. value λ_{max} = 439 nm

HOMO   97 % contribution   LUMO
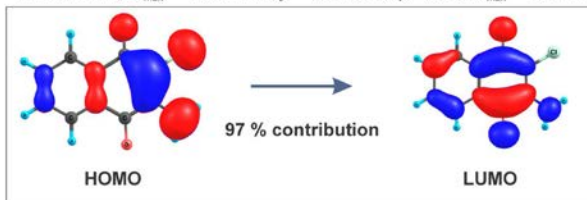
Transition at λ_{max} = 346.1 nm, f = 0.079. Exp. value λ_{max} = 332 nm

HOMO-1   96% contribution   LUMO

Transition at λ_{max} = 310.1 nm, f = 0.169. Exp. value λ_{max} = 287 nm

HOMO-3   89 % contribution   LUMO

Transition at λ_{max} = 270.6 nm, f = 0.316. Exp. value λ_{max} = 265 nm

HOMO   92 % contribution   LUMO+1
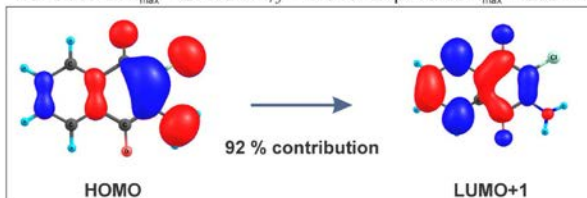
Figure S34. Molecular orbitals of **6** involved in the four lowest energy electronic transitions (contour values plotted at 0.03 (e/Bohr^3)$^{1/2}$).
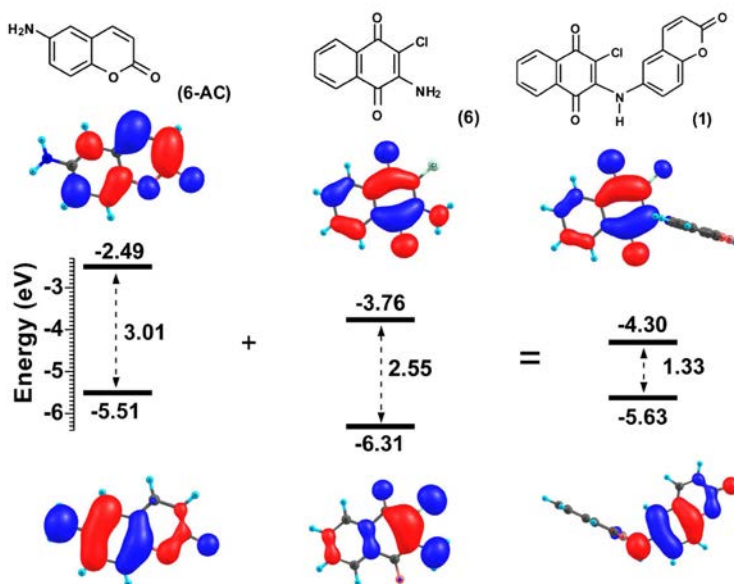
Figure S35. Molecular orbital diagrams for 6-AC, **6** and conjugate **1** in the excited state (contour values plotted at 0.03 (e/Bohr^3)$^{1/2}$).